JCB Journal of Cell Biology

ARTICLE

ER–plasma membrane contact sites deliver ER lipids and proteins for rapid cell surface expansion

Madison Smith[1], Lincoln Gay[1], and Markus Babst[1]

As a consequence of hypoosmotic shock, yeast cells swell rapidly and increase the surface area by ∼20% in 20 s. Approximately, 35% of this surface increase is mediated by the ER–plasma membrane contact sites, specifically the tricalbins, which are required for the delivery of both lipids and the GPI-anchored protein Crh2 from the cortical ER to the plasma membrane. Therefore, we propose a new function for the tricalbins: mediating the fusion of the ER to the plasma membrane at contact sites. This proposed fusion is triggered by calcium influx via the stretch-gated channel Cch1 and is supported by the anoctamin Ist2.

Introduction

Unlike organelle membranes, the plasma membrane (PM) of eukaryotic cells is under substantial tension because of turgor pressure and mechanical forces that exert lateral tension on the membrane (e.g., interactions with the extracellular matrix in tissue) (Pontes et al., 2017; Le Roux et al., 2019). This membrane tension has to be maintained within physiological range to ensure proper function of the PM and its associated proteins. High tension affects membrane properties by decreasing lipid packing and thus increasing fluidity. As a consequence, membranes become thinner, less organized, and show partial loss of the barrier function. This increase in lipid fluidity of the high-tension PM partially mimics the effects observed by the presence of surfactants or high temperatures. High PM tension can occur as a consequence of an imbalance in secretion and endocytosis or changes in cell surface-to-volume ratios. Examples are deformations caused by mechanical stress or cell migration and changes in osmolarity. Cells are able to adjust membrane tension by adding or removing lipids and proteins from the cell surface or by changing cytoplasmic osmolarity. Therefore, tension is a controllable parameter that allows cells to counteract the environmental effects on PM fluidity that are beyond the control of the cell (e.g., surfactants and temperature).

Even though PM tension is recognized as a key parameter that affects most PM-associated functions, the sensing of PM tension and the mechanisms for maintaining proper tension are mostly unknown. Current knowledge is mainly limited to specialized mammalian cell types that repeatedly undergo large surface area changes, like muscle cells that use caveolae as PM reservoirs (Parton, 2018), and umbrella cells of the uroepithelium that house specialized vesicles that can provide or store membrane (Apodaca, 2004). In unicellular organisms such as the yeast *Saccharomyces cerevisiae*, where PM tension control is particularly important to adjust to rapid and dramatic environmental changes, surprisingly little is known about how these cells maintain physiological PM tension.

One system that has been implicated in the regulation of yeast PM tension utilizes eisosomes, which are ∼50 nm deep and ∼300 nm long furrows of the PM that have functional similarities to caveolae in vertebrates (Douglas and Konopka, 2014). Eisosomes respond to high membrane tension by flattening (Appadurai et al., 2020), which can provide some surface area to counter the high tension. Furthermore, eisosome-localized Slm1 and Slm2 proteins redistribute during high PM tension and bind to the TORC2 kinase complex. As a consequence, TORC2 activates a signaling pathway that leads to an upregulation of sphingolipid synthesis in the ER. This eisosome-Slm1/2-TORC2 signaling pathway is proposed to maintain PM homeostasis (Berchtold et al., 2012). However, this system requires transport of newly synthesized sphingolipids via the secretory pathway to the PM and therefore is not able to respond rapidly to changes in PM tension.

Previously, we observed rapid swelling of hypoosmotic-treated yeast, which resulted in an increase in surface area by ∼20% (Appadurai et al., 2020). Eisosome flattening and stretching of the existing PM can only account for approximately half of this cell surface expansion. Therefore, we started the search for an additional mechanism that would allow the cell to respond to high PM tension and rapidly expand without losing cell integrity. Interestingly, we found that high PM

[1]Henry Eyring Center for Cell and Genome Science, University of Utah, Salt Lake City, UT, USA.

Correspondence to Markus Babst: babst@biology.utah.edu.

tension causes the rapid delivery of cortical ER lipids and proteins to the PM, which suggests a membrane fusion mechanism.

Results

In a previous study, we visualized yeast under different stress conditions using a microfluidics chamber combined with fluorescence microscopy (Moharir et al., 2018). This chamber maintains optimal growth conditions during the imaging of yeast and allows for rapid change of environmental parameters. Most importantly, microfluidics chambers allowed us to follow the same cells over time, which eliminated cell-to-cell variability issues. One surprising result from these experiments was that most environmental stress conditions resulted in rapid cell size changes (Appadurai et al., 2020). This indicated that the yeast cell wall is not a rigid structure, but allows for cell volume changes. As a consequence of these volume adjustments, the cell surface area changes, which begs the question: how does yeast maintain proper PM function, particularly during acute swelling of the cell?

To answer this question, we exposed yeast to a hypoosmotic shock by growing the cells in the presence of 1 M sorbitol and then switching these cells in the microfluidics system to a growth medium without sorbitol. In the presence of 1 M sorbitol, yeast adjusts its intracellular osmolarity by synthesizing and storing glycerol. When switched to a sorbitol-free medium, the high intracellular osmolarity will cause water influx through aquaporins, causing the swelling of the cell. This osmotic stress opens the aquaglyceroporin Fps1 and causes the subsequent release of the stored glycerol into the environment (reviewed in Hohmann [2002]). As a result of both water influx and glycerol efflux, the turgor pressure of the cell rapidly returns to normal.

The wild-type yeast strain used for the hypoosmotic stress experiments expressed a cytoplasmic mCherry-pHluorin fusion protein that allowed us to visualize both the cell size change and the changes in cytoplasmic pH by fluorescence microscopy. Because yeast acidifies the growth medium to ∼pH4, a loss in cell integrity would be indicated by a dramatic drop in pHluorin signal, whereas mCherry fluorescence would not be affected. We took pictures of ∼100 cells before and after 2–3 min of hypoosmotic shock. Using these images, we determined the cell size changes of the mother cells by measuring the short and long diameters of the ellipsoid cells. We also measured the size changes of the growing bud in cases where the bud was at least 1.5 µm in diameter. These measurements showed that swelling increases both axes of the mother cells similarly, resulting in a median increase in cell surface area of ∼19% (Fig. 1, A and B). Budding cells swelled similarly, exhibiting a median surface increase of ∼17% (Fig. 1 B). These dramatic increases in cell size occurred in most cases without loss of cell integrity. Out of 109 cells total, we observed only 1 dramatic loss of pHluorin signal, indicating cell lysis ("lysed" in Fig. 1 C). Furthermore, only two other cells were found to have ruptured both the PM and the cell wall, resulting in the leaking of cytoplasm (loss of both pHluorin and mCherry signal; "ruptured" in Fig. 1 C). In summary, these data indicated that yeast is able to rapidly increase cell surface area with only minor loss of cell integrity.

The ER–PM contact sites are involved in rapid cell expansion

To gain insight into the mechanism supporting the rapid cell surface expansion, we took a candidate approach by measuring the surface area changes of a set of yeast mutants that might be defective in maintaining PM integrity. As before, we switched these cells in the microfluidics system from a growth medium containing 1 M sorbitol to a growth medium without sorbitol. For simplicity, we only measured a randomly chosen diameter for each mother cell and assumed a spherical shape for the surface calculations. For the wild-type cells, these simplified measurements indicated a surface increase of ∼16%, slightly less than the ∼19% determined with the previous method (compare Fig. 1 D with Fig. 1 B). As an additional control, we measured the cell size increase of *fps1*Δ, a strain deleted for the aquaglyceroporin that functions in the rapid secretion of glycerol during hypoosmotic shock (Luyten et al., 1995). Without glycerol secretion, the cells experience a stronger turgor pressure when shifted to a low osmolarity medium. As a consequence, after 2 min of hypoosmotic shock, *fps1*Δ cells exhibited a cell surface increase larger than observed with wild type (18.3% versus 16.1%; Fig. 1 D). Furthermore, the lack of glycerol secretion also affected the survival of hypoosmotic-shocked cells: the number of lysed or ruptured cells increased to 25% from 3% in wild-type cells (Fig. 1 C).

We expected that loss of eisosomes would affect cell surface expansion since a previous study observed flattening of the eisosomal membrane furrows under high PM tension (Appadurai et al., 2020). Consistent with this idea, we found that loss of the eisosome component Pil1 reduced cell surface expansion by ∼5% (*pil1*Δ in Fig. 1 D).

Another set of factors we identified with the candidate approach as being important for cell expansion were proteins of the ER–PM contact sites (EPCS). In yeast, most of the ER is found in close proximity to the PM where it underlies ∼40% of the PM (West et al., 2011). This cortical ER (cER) is physically linked to the PM by EPCS proteins which keep the two membranes within a ∼22 nm distance (Fernandez-Busnadiego et al., 2015). EPCS proteins are anchored in the ER membrane and connect to the PM by binding either to anionic lipids or to proteins of the PM (Eisenberg-Bord et al., 2016; Gatta and Levine, 2017). Key proteins of the EPCS are the three tricalbins Tcb1/2/3 (also referred to as extended synaptotagmins), the proposed calcium-regulated chloride channel Ist2 and the two homologous VAPs (VAMP Associated Protein) Scs2 and Scs22. The EPCS proteins are evolutionarily conserved and thus are likely to perform similar functions in all eukaryotes. However, what these important functions are is not well understood. Studies both in yeast as well as in mice have shown that loss of the three tricalbins resulted in mild to no observable phenotypes, respectively (Sclip et al., 2016; Tremblay and Moss, 2016; Thomas et al., 2022). However, the hypoosmotic stress assay indicated that the EPCS mutants *tcb2/3*Δ and *ist2*Δ showed a 5–6% reduction in cell surface expansion (Fig. 1 D; the *tcb2/3*Δ double mutant causes a loss of tricalbin function), a phenotype that was additive with the *pil1*Δ defect (*tcb2/3*Δ*pil1*Δ; Fig. 1 D). The remaining ∼5% of the cell surface increase of the *tcb2/3*Δ*pil1*Δ mutant was likely provided by stretching of the existing membrane (Le Roux et al., 2019).

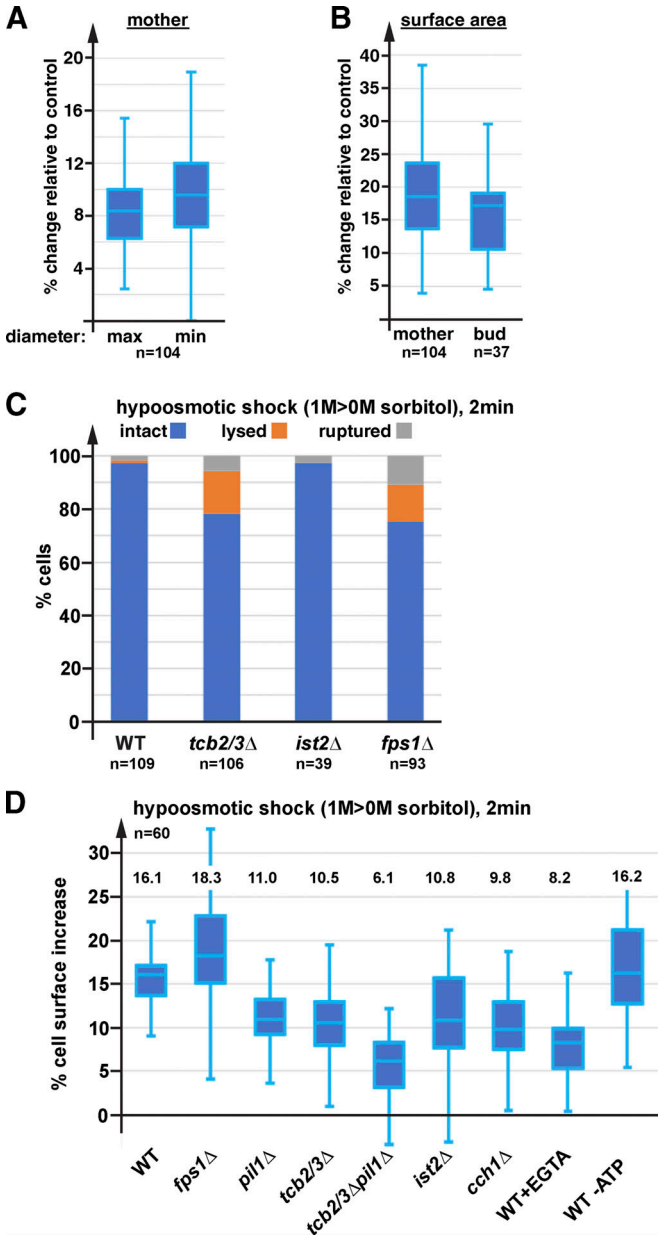

Figure 1. **Hypoosmotic shock causes rapid cell swelling and surface expansion. (A and B)** Wild-type cells expressing pHluorin-mCherry (SEY6210 containing pMB517) were grown in SD_{-URA}+1 M sorbitol, flushed into a microfluidics chamber, and shifted to a growth medium without sorbitol. Fluorescence microscopy pictures from cells before treatment and the same cells 2 min after hypoosmotic shock were used to measure changes in the maximal and minimal diameter of the ellipsoidal cells (A). The resulting calculated changes in surface area are shown in B. **(C)** Wild type, *tcb2/3Δ*, *ist2Δ*, and *fps1Δ* cells expressing pHluorin-mCherry (SEY6210, MTY18, MTY2, and LGY83 containing pMB517) were exposed in a microfluidics chamber to a hypoosmotic shock (1 M sorbitol > 0 M sorbitol), and the observed changes in morphology and pHluorin/mCherry fluorescence were used to determine the number of lysed cells (loss of pHluorin signal, indicating loss of PM integrity) and ruptured cells (loss of pHluorin and mCherry signal, indicating ruptured cell wall and PM). **(D)** Strains expressing Nce102-mCherry (AMY4, MTY81, MTY55, MTY52, MTY83, MTY47, and MTY68) were hypoosmotic-shocked in a microfluidics chamber and the cell surface change was determined based on changes of a specified diameter. For the EGTA treatment, the growth medium contained 10 mM EGTA. To deplete ATP, 5 mM NaN_3 and 5 mM NaF were added to the cells 5 min before treatment (WT -ATP). The graphs in A, B, and D are box-and-whisker plots, indicating the mean.

Tricalbin mutants exhibit increased cell lysis during hypoosmotic shock

We performed a detailed analysis of the *tcb2/3Δ* mutant compared with the wild type. During the time-lapse imaging of hypoosmotic shocked cells, we monitored changes in the cytoplasmic pH and cell size. Fig. 2, A–C shows representative examples of the observed changes and Fig. 2 D summarizes the quantification of 20 movies. After an ∼30 s delay, which was the time it took for the hypoosmotic growth medium to reach the cells, wild type showed rapid cell surface expansion of ∼1%/s (blue line in Fig. 2 A). Halfway through cell swelling, the cytoplasmic pH showed a small drop indicated by a slightly lower pHluorin/mCherry ratio, followed by a temporary increase in pH (green line in Fig. 2 A; quantified in Fig. 2 D). Since the pHluorin/mCherry measurements were not calibrated, we are not able to directly convert these values into pH changes. However, previous flow cytometry experiments using the same pH sensor showed that the drop from pH7 to pH6 was accompanied by a ∼35% loss in pHluorin/mCherry ratio (Moharir et al., 2022), suggesting that the observed fluctuations were <1 pH unit. The reason for these pH changes is not obvious and will be discussed below.

In comparison with wild type, the *tcb2/3Δ* mutant strain exhibited a large cell-to-cell variability in cell expansion (three different examples are shown in Fig. 2 C). Although surface expansion kinetics were similar to wild type (∼1%/s), the extent to which these cells expanded varied more dramatically than observed in wild type (Fig. 2 D). Furthermore, whereas wild type mostly maintained its size at the level of the maximal extension (∼2% drop at 100 s), the cell surface area of *tcb2/3Δ* shrunk on an average by 6% after reaching its peak (Δsurface; Fig. 2, C and D). This collapse of cell size can explain the ∼5% reduced cell expansion observed with *tcb2/3Δ* ∼2 min after hypoosmotic shock (Fig. 1 D). It should be noted that because of these size changes, we extended the analysis to 120 s for each of the mutants. However, to stay consistent with wild type, the Δsurface values were all measured at 100 s.

Unlike wild type, the *tcb2/3Δ* mutant cells showed a much more pronounced pH drop during acute hypoosmotic shock (Fig. 2, C and D). Because the pH of the growth medium is ∼4, we suggest that the observed drop in cytoplasmic pH is caused by a partial loss of PM barrier function in these mutant cells. Fig. 2 C shows two examples of cells where after an initial pH drop and partial recovery, the cells exhibited a collapse of the pHluorin signal, which suggested lysis of the PM. Consistent with this idea, we observed a concomitant reduction in cell size (see arrows in Fig. 2 C), suggesting a sudden drop in turgor pressure. Surprisingly, lysed cells were able to restore normal cytoplasmic pH within <5 min (as shown for the third example of Fig. 2 C), which suggested that these cells were able to repair the lysed PM and remain viable. We confirmed this observation using a simple viability assay on agar plates. The colony count of the cells before and after a hypoosmotic shock indicated no obvious loss of viability of *tcb2/3Δ* (Fig. 2 E).

Quantification of ∼100 cells indicated that ∼16% of the *tcb2/3Δ* mutants lysed (Fig. 1 C; loss of pHluorin signal as shown in two examples in Fig. 2 C). In addition, ∼6% of *tcb2/3Δ* cells

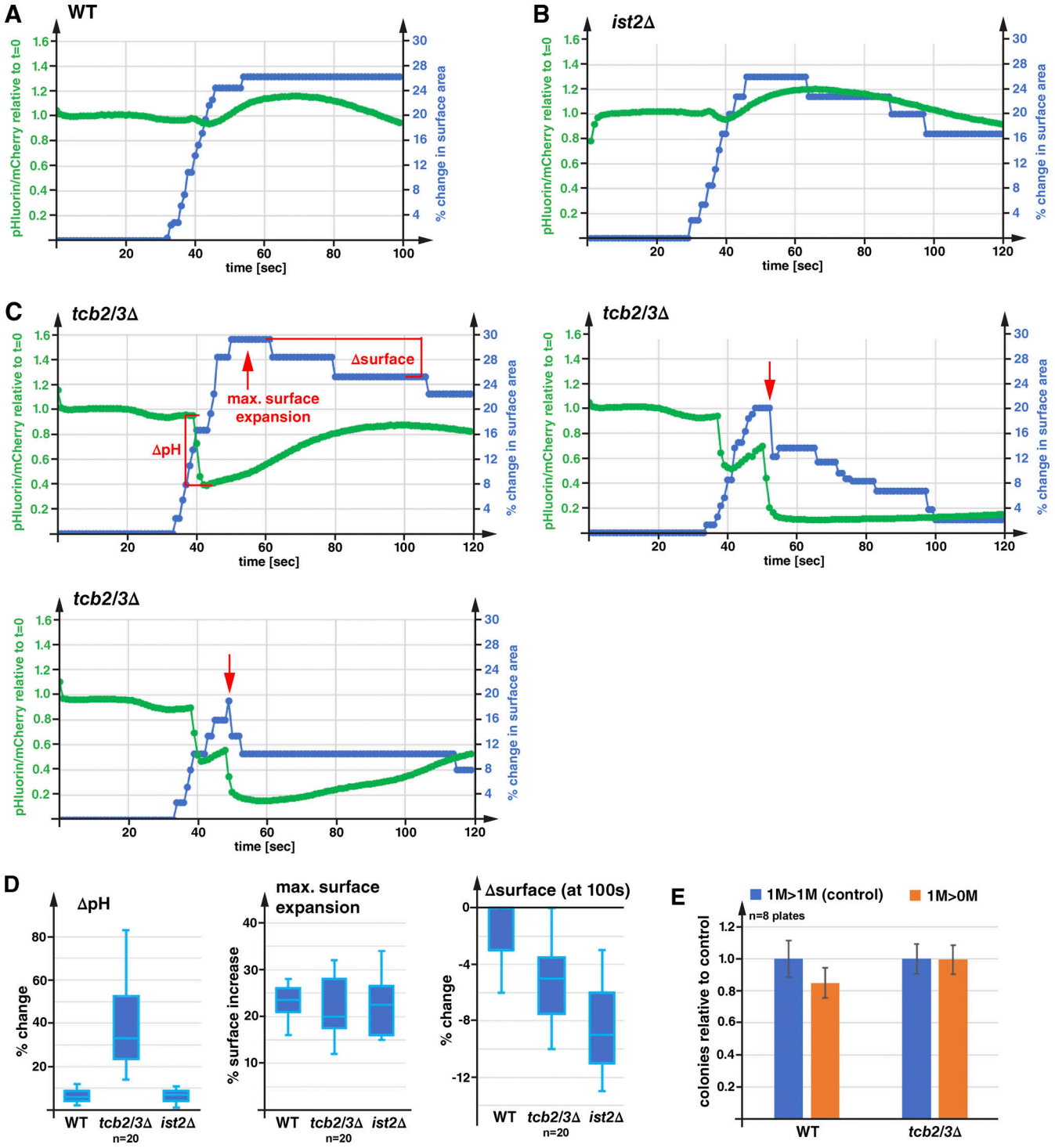

Figure 2. **During hypoosmotic swelling, tricalbin mutants lose cell integrity. (A–C)** Using time-lapse imaging, wild type and mutant strains expressing pHluorin-mCherry (SEY6210, MTY2, and MTY18 containing pMB517) were observed during exposure to hypoosmotic conditions (1 M sorbitol > 0 M sorbitol). The resulting movies were analyzed for cell surface changes and changes in cytoplasmic pH (pHluorin/mCherry ratio). Downward arrows in C mark cell lysis events. **(D)** Quantification of the data obtained by the time-lapse imaging presented in box-and-whisker plots (line indicates the mean). The first panel in C explains the measured parameters. **(E)** Wild type (SEY6210) and tricalbin mutant (MTY18) cells were either moved to the same sorbitol-containing medium (1 M sorbitol > 1 M sorbitol) or exposed to a hypoosmotic shock (1 M sorbitol > 0 M sorbitol) at 30°C. 5 min after treatment, the cells were plated and colonies were counted after 2 days of growth.

ruptured (loss of both pHluorin and mCherry; Fig. 1 C), and these cells did not recover. However, the plate assay shown in Fig. 2 E seemed not sensitive enough to capture this small percentage of cell loss. In comparison, wild type exhibited only 2–3% loss of cell integrity (Fig. 1 C). This phenotype of the hypoosmotic treated *tcb2/3*Δ mutant was similar in severity to the phenotype observed with a strain deleted for Fps1, the aquaglyceroporin that allows for the rapid release of glycerol (Fig. 1 C).

Together, the microfluidics analyses suggested that during hypoosmotic shock, wild-type yeast cells rapidly swell and maintain this enlarged size. We hypothesize that the cells are able to maintain this size because of the added membrane to the cell surface. In contrast, *tcb2/3*Δ cells seem to be defective in membrane addition and thus these cells experience lysis during the swelling and cell shrinking after normal turgor pressure has been restored. This rather dramatic phenotype of the *tcb2/3*Δ mutants was intriguing and suggested a specific role for the tricalbins in response to acute membrane stress.

The data we obtained from microfluidics microscopy experiments were supported by flow cytometry analyses of wild type and mutant cells expressing the same pHluorin-mCherry construct. We grew the cells in the presence of 1 M sorbitol and switched them either to the same growth medium (1 M > 1 M) or to a medium lacking sorbitol (1 M > 0 M sorbitol). We analyzed ∼200,000 cells of each treatment by flow cytometry and determined the pHluorin/mCherry ratio of each cell (Fig. 3). To simplify the data analysis, we defined two groups of cells. One group was defined by having a pHluorin/mCherry ratio <1, which suggested a very low cytoplasmic pH and thus was labeled "lysed." The second group was defined by having a pHluorin/mCherry ratio >1 but smaller than the 95% line set by the control sample (Fig. 3 A). This group of cells exhibited an obvious pH drop possibly caused by partial loss of PM barrier function, but they did not lose cell integrity and thus was labeled "low pH." Because the gating of the flow cytometry data removed cells with low mCherry signal, we were not able to quantify the number of ruptured cells (cells that spilled their cytoplasm). Using this data analysis, we observed with hypoosmotic shocked wild type an increase in the number of low pH cells from 4% (con) to ∼20% (Fig. 3 D), which likely corresponded to the small pH drop observed by the microfluidics experiments in Fig. 2 A. Furthermore, we found a slight increase from ∼0.5% to 3% in the lysed-cell population (Fig. 3 D). In contrast, the *tcb2/3*Δ cells exhibited dramatic increases in both the lysed and the low-pH groups. Combined, close to 90% of these mutant cells showed a clear acidification phenotype (Fig. 3, C and D), a phenotype that was more severe than observed for the *fps1*Δ mutant (Fig. 3, B and D). Together, the flow cytometry experiments supported the notion that in the absence of the tricalbins, yeast is not able to expand the PM safely and thus experiences loss of cell integrity during hypoosmotic shock.

Ist2 is not essential for rapid cell surface increase during hypoosmotic stress

In contrast to the tricalbin mutant, deletion of the EPCS protein Ist2 resulted in a much less severe phenotype. Although the defect in hypoosmotic cell expansion of *ist2*Δ was similar in severity to that observed with *tcb2/3*Δ (Fig. 1 D; and Fig. 2, B and D), we observed no increase in cell lysis during hypoosmotic stress (Fig. 1 C) and no pronounced pH drop during the acute phase of cell swelling (Fig. 2, B and D). Similarly, the flow cytometry analysis indicated only a minor increase in the *ist2*Δ population with a low pHluorin/mCherry ratio (Fig. 3 D). We were able to explain the difference between the two EPCS mutants by the observation that unlike *tcb2/3*Δ, *ist2*Δ mutants were able to slowly increase in cell size during hypoosmotic stress (Fig. 4). This observation suggested that Ist2 is not essential for the EPCS-mediated cell expansion but might play a role in the efficiency of this stress pathway.

Microscopy of the VAP double mutant, *scs2*Δ*scs22*Δ, showed dramatic cell morphology phenotypes (elongated cells with defective budding patterns; not shown), which indicated defects in polarized secretion and cell wall synthesis. This pleiotropic phenotype can be explained by the broad functions of the VAPs at various membrane contact sites (Scorrano et al., 2019). Because of these complications, we decided not to include the VAP mutants in our analyses.

In summary, the data so far indicated that the tricalbins play an important role in rapid cell expansion and the survival of yeast during hypoosmotic stress. This phenotype of the tricalbin mutants is not linked to the tethering function of these proteins since the loss of Ist2, a protein that plays a more dominant role in cER-PM tethering (Manford et al., 2012), exhibited only minor defects. Instead, we propose that during acute hypoosmotic stress, the tricalbins provide membrane to the PM, which allows the cell to safely swell to its full extent without jeopardizing cell integrity.

The cortical ER provides membrane for the rapid expansion of spheroplasts

The hypoosmotic-induced expansion of the cell surface is limited by the cell wall and reached a median of ∼16–19% (Fig. 1, B and D). Curiously, the maximum observed surface expansion was much higher at 38% (Fig. 1 B). To push the system and determine if the yeast PM could expand even further without losing cell integrity, we spheroplasted yeast cells expressing an ER-localized superfolder pHluorin (ER-pHluorin) and a tagged eisosome marker, Nce102-mCherry. The eisosome marker allowed us to identify the properly spheroplasted cells (spheroplasts exhibit large eisosomes; see arrow in Fig. 5 A) and the observed loss of eisosome structures served as an indicator for high PM tension. The removal of the cell wall was performed at pH 6.5 and in the presence of 0.4 M sorbitol to minimize turgor pressure. These spheroplasts were then flushed into the microfluidics chamber and imaged by fluorescence microscopy before and after shift to 0.1 M sorbitol. This hypoosmotic shock caused the spheroplasts to expand dramatically, resulting in a median increase in surface area of ∼54% (Fig. 5, A and C). Time-lapse imaging of the spheroplast expansion indicated a rate of ∼1% surface area increase per second, which was similar to the expansion rate of walled cells (compare Fig. 5 B with Fig. 2 A; see Video 1). During expansion, the ER-pHluorin signal declined only slightly (see Video 1 and micrographs in Fig. 5 B), suggesting that cell integrity remained intact. However, ∼9% of the

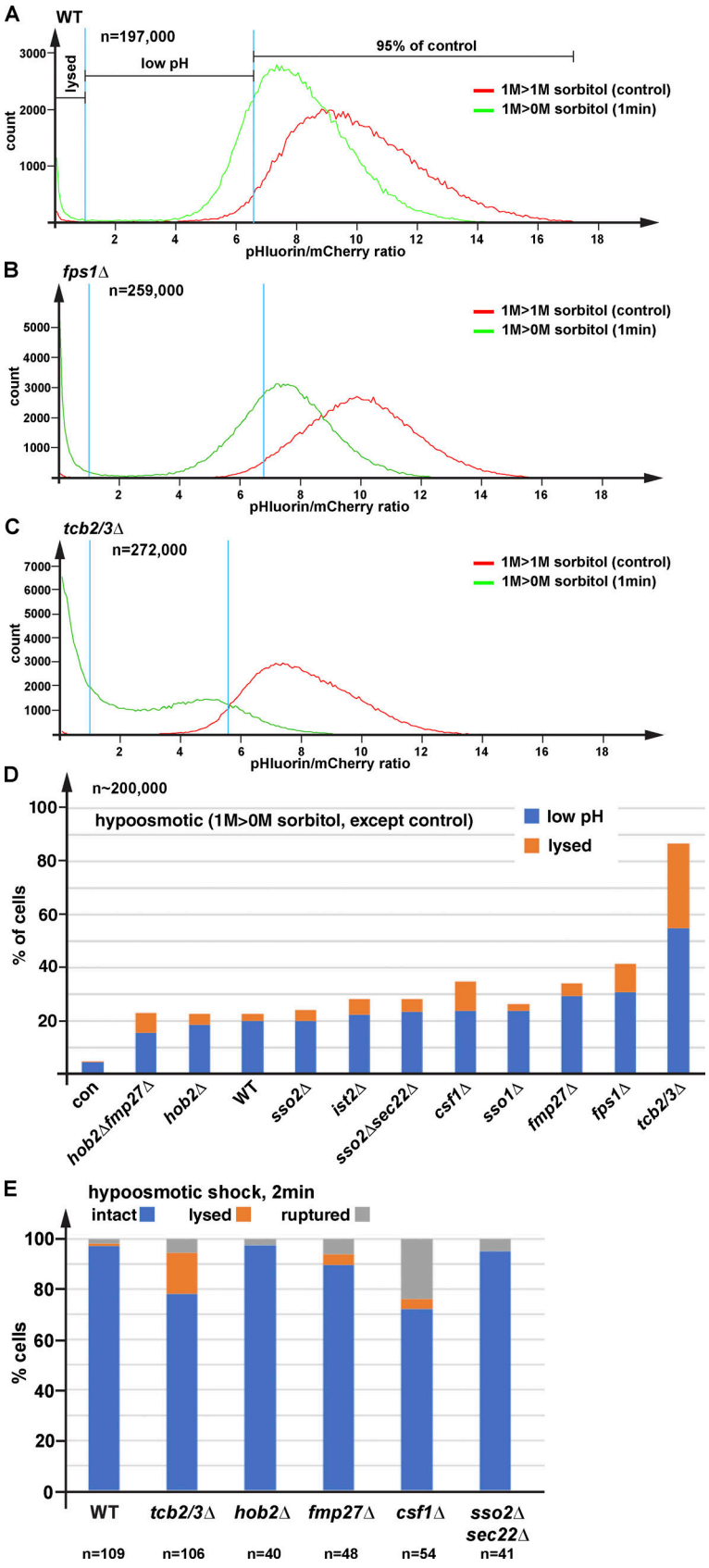

Figure 3. **Flow cytometry-based analysis of cell integrity after hypoosmotic shock.** Wild-type and mutant strains expressing pHluorin-mCherry (SEY6210, LGY83, MTY18 containing pMB517) were grown in the presence of 1 M sorbitol. The cells were either switched to a new medium containing sorbitol (control; 1 M sorbitol > 1 M sorbitol) or to medium without sorbitol (hypoosmotic shock; 1 M sorbitol > 0 M sorbitol) and within ∼1 min analyzed by flow cytometry. **(A–C)** The plots show the distribution of the pHluorin/mCherry ratio of ∼200,000 cells (readout of cytoplasmic pH). **(D)** Quantitative analysis of the flow cytometry data collected from wild-type and mutant strains expressing pHluorin/mCherry (MTY93, MTY89, SEY6210, MTY7, MTY2, MTY86, MTY91, MTY11, STY11, LGY83, and MTY18 containing pMB517). "Lysed" cells were defined as cells with a pHluorin/mCherry ratio <1 (indicating loss of PM integrity), whereas "low pH" cells showed a pHluorin/mCherry ratio that was <95% of the control cells but >1 (see panel A). Based on this analysis, the controls of all strains were very similar (shown as "con"). **(E)** Wild-type and mutant yeast strains expressing pHluorin-mCherry (SEY6210, MTY18, MTY89, STY11, MTY91, MTY86 containing pMB517) were monitored during hypoosmotic shock (1 M sorbitol > 0 M sorbitol) in a microfluidics chamber to determine the percentage of cell lysis (loss of pHluorin signal, indicating loss of PM integrity) and cell rupture (loss of pHluorin and mCherry signal, indicating ruptured cell wall and PM; see Fig. 1 C). The wild type and *tcb2/3*Δ data are identical to those shown in Fig. 1 C.

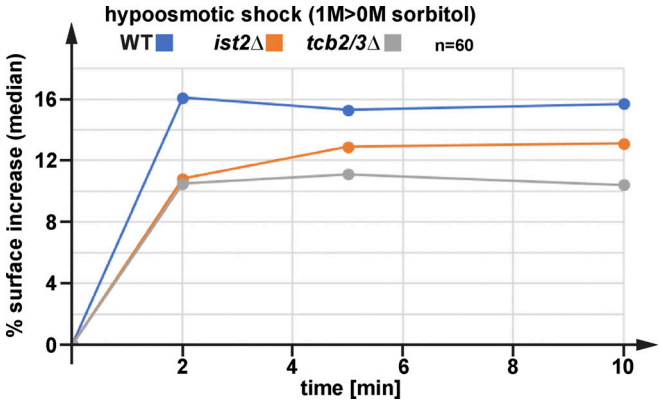

Figure 4. **Deletion of *IST2* resulted in delayed cell expansion.** Hypoosmotic-induced changes in cell surface area were measured from wild-type and mutant strains (AMY4, MTY47, MTY52) as described in Fig. 1 D (the 2 min time points are the data set shown in Fig. 1 D).

wild-type spheroplasts ruptured during these experiments (Fig. 5 D).

During spheroplast swelling, the ER exhibited rapid movement and morphology changes (see Video 1). After hypoosmotic shock, most of the cER sheets were lost and the remaining cER appeared mainly tubular (Fig. 5, A and F). In total, we determined that the cER lost ∼35% of its surface area (Fig. 5 G; based on the ER changes observed at the spheroplast surface closest to the microscope objective, as shown in Fig 5, A and F). We also observed changes in the nuclear membrane. In spheroplasts containing two connected nuclei (mother and daughter nuclei of G2 cells), the nuclei fused back together and formed a single structure with reduced surface area (see nuclear membrane in Fig. 5 A). This observation suggested that these spheroplasts not only lost cER but also membranes from other parts of the ER network. Together, the data indicated that most of the membrane required for the dramatic spheroplast expansion was provided by the ER (cER has approximately the same surface area as the PM; [Manford et al., 2012]). In addition, eisosome flattening and PM stretching likely supported some of the surface expansion.

As observed with walled cells, spheroplast expansion during hypoosmotic conditions was dependent on the tricalbins. 75% of *tcb2/3Δ* spheroplasts did not expand but ruptured during the hypoosmotic shock (recognized by reduced cell size, collapsed cER, and extracellular PM remnants; Fig. 5 E). The remaining 25% that survived the hypoosmotic shock exhibited a wide range of expansion, resulting in cell surface changes from as little as 10% to as much as 100% (compared to 39–66% in wild type; Fig. 5 C). Overall, the median of the surface area changes of the surviving *tcb2/3Δ* spheroplasts was half of that observed with wild-type cells (Fig. 5 C). However, the few surviving *tcb2/3Δ* spheroplasts we were able to analyze (sufficiently expressed ER-pHluorin) showed ∼40% loss of cER, which was similar to the loss observed for wild-type spheroplasts (Fig. 5 G). Together, our observations indicated that the tricalbins are important for the large, hypoosmotic-induced delivery of cER membrane to the surface of spheroplasts, even though some mutant cells seem to be able to bypass this requirement.

On average, the *ist2Δ* mutant spheroplasts expanded their surface area to a similar extent as wild type (∼51%, Fig. 5 C), supporting the idea that Ist2 is not essential for the rapid cell expansion. However, the measurements also indicated that the extent of spheroplast swelling was not as consistent as observed with wild type and the loss of cER was less severe in *ist2Δ* (Fig. 5 G), suggesting problems with the cER-to-PM membrane transfer.

Together, the spheroplast analysis identified cER as the main membrane source for PM expansion and further supported the importance of the tricalbins in preventing cell lysis/ruptures during the acute phase of hypoosmotic stress.

cER-PM membrane transfer causes phosphatidylserine (PS) exposure

At the PM, the negatively charged phospholipid PS localizes exclusively to the cytoplasmic leaflet, whereas at the ER, PS is found in both leaflets (Tsuji et al., 2019). Therefore, the cER–PM membrane transport might disrupt PS asymmetry at the cell surface. We tested this idea by spheroplasting yeast expressing the eisosome marker Nce102-mCherry and exposed these spheroplasts to a hypoosmotic shock. After 2 min at low osmolarity, we added fluorescently labeled PS-binding protein annexin-V to the swollen spheroplasts and visualized these cells by fluorescence microscopy. It should be noted that these experiments were not performed in a microfluidics system and thus the hypoosmotic stress conditions had to be adjusted (switch spheroplasts from 0.8 to 0.1 M sorbitol in a test tube). The images of these experiments showed that hypoosmotic shock caused a dramatic increase in annexin-V staining of the spheroplasts, suggesting that the cER-PM membrane transfer disrupted PS asymmetry at the PM (Fig. 6 A; quantified in Fig. 6 C). Unlike cell debris, the swollen but intact spheroplasts exhibited punctate annexin-V staining, which suggested a clustering of the surface-exposed PS in these spheroplasts (compare Fig. 6 A with Fig. 6 B). The reason for this PS clustering is not known.

After hypoosmotic shock, the *ist2Δ* mutant spheroplasts also exposed PS on the surface, although to a lesser degree (Fig. 6, A and C). This finding fit to the other phenotypes observed with this mutant, which suggested not a block but a delay or inefficiency of the cER to PM membrane transfer. The fact that deletion of *IST2* does not block PS exposure is particularly interesting since Ist2 belongs to the family of TMEM16/anoctamin proteins that have been implicated in the loss of PS asymmetry during platelet activation (blood coagulation) and apoptosis (Falzone et al., 2018).

Calcium influx plays an important role in the EPCS-mediated membrane transfer

Published data suggested that calcium is a likely regulator for the cER-to-PM membrane transfer. The tricalbins contain calcium-binding C2 domains that regulate their interactions with the PM (Schulz and Creutz, 2004) and Ist2 is predicted to be a calcium-regulated chloride channel (Kunzelmann et al., 2016). We found that mutations of the PM calcium channel Cch1 impair cell expansion (Fig. 1 D). Furthermore, it has been shown that

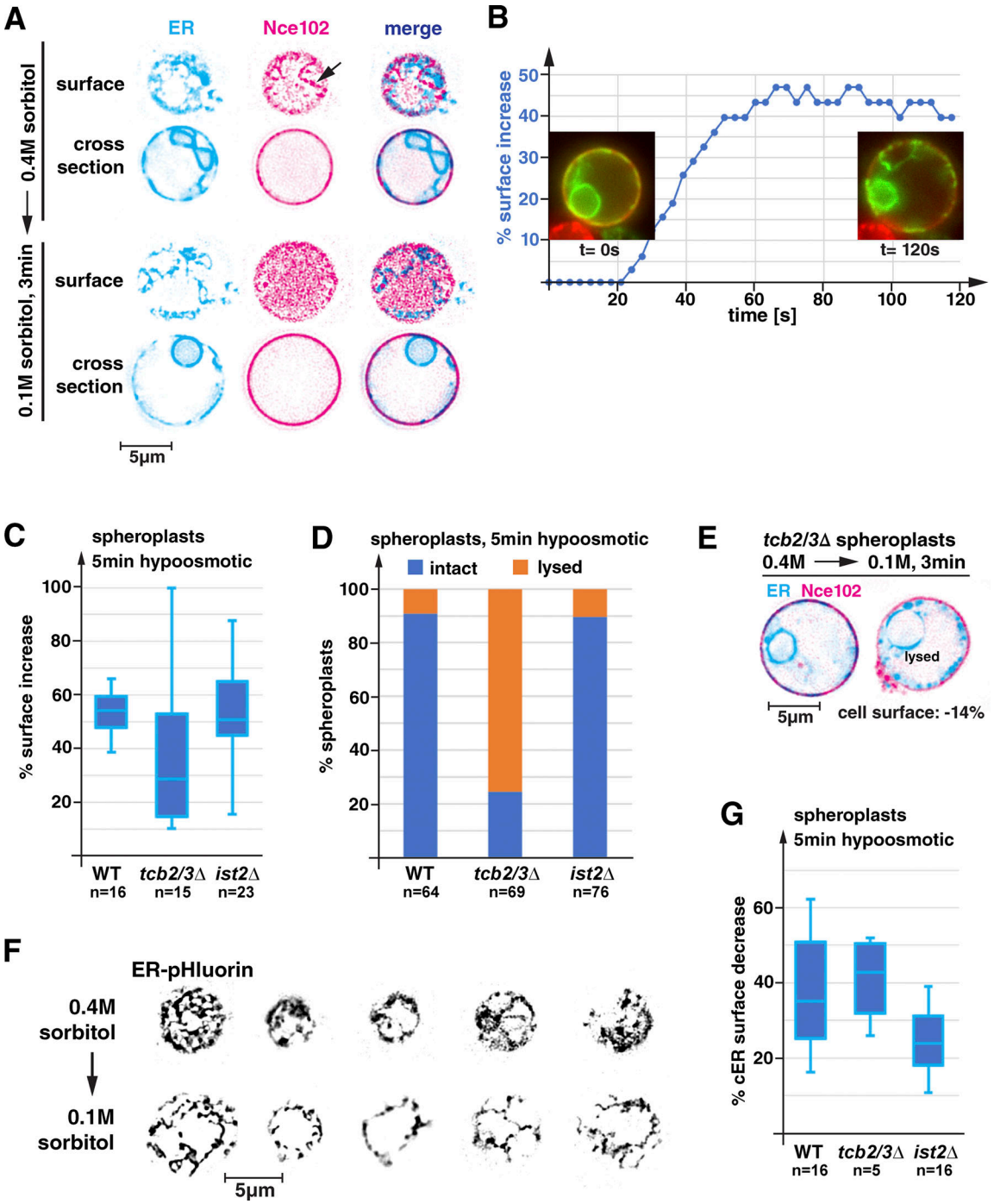

Figure 5. **Hypoosmotic-induced spheroplast expansion results in cER loss. (A)** Spheroplasted wild-type cells expressing ER-pHluorin and Nce102-mCherry (AMY4 containing MRV66) were flushed into a microfluidics chamber in the presence of 0.4 M sorbitol and then switched to a medium containing 0.1 M sorbitol. The arrow indicates an enlarged eisosome that is commonly observed in spheroplasts. **(B)** Analysis of time-lapse imaging of spheroplast swelling (AMY4 containing MRV66). The corresponding movie can be found in Video 1 (video is 3× sped up). **(C)** Quantification of the surface increase observed with hypoosmotic treated wild-type and mutant spheroplasts (AMY4, MTY52, and MTY47 containing MRV66). **(D)** Quantification of the number of cells that lysed (loss of PM integrity) during hypoosmotic-induced cell expansion (0.4 M sorbitol > 0.1 M sorbitol). **(E)** Example of a *tcb2/3*Δ spheroplast (MTY52 containing MRV66) that lysed during hypoosmotic shock. **(F)** Five examples of wild-type cells expressing ER-pHluorin as an ER marker, before and after the hypoosmotic shock (0.4 M > 0.1 M sorbitol). The microscopy pictures show the surface of the cell, which visualizes cER. **(G)** Quantification of the change in cER surface caused by hypoosmotic spheroplast expansion. The graphs in C and G are box-and-whisker plots, indicating the mean.

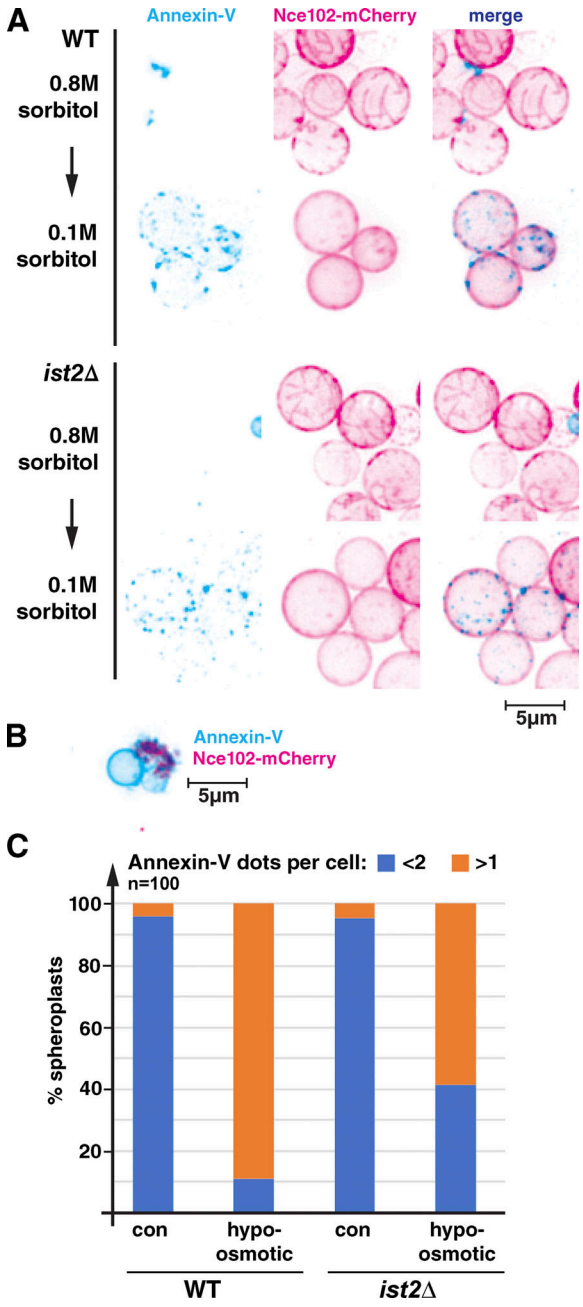

Figure 6. **Hypoosmotic swelling of spheroplasts causes PS exposure. (A)** Wild-type and *ist2*Δ cells (AMY4, MTY47) were spheroplasted in presence of 0.8 M sorbitol. After hypoosmotic shock in 0.1 M sorbitol medium, the spheroplasts were stained with annexin-V that binds to surface exposed PS. **(B)** Example of cell remnants stained with annexin-V. **(C)** Quantification of the annexin-V staining.

hypoosmotic shock causes a spike in intracellular calcium (Batiza et al., 1996), an observation we confirmed using yeast expressing GCaMP (Fig. 7 A). Deletion of *CCH1* resulted in a reduced calcium response to the hypoosmotic shock (Fig. 7 A), implicating other calcium sources in the response, such as the vacuole and mitochondria. However, based on the reduced cell expansion of *cch1*Δ (Fig. 1 D), we propose that calcium influx via Cch1 is locally triggering the EPCS-mediated membrane transfer and that other calcium sources are not relevant for this response. In support of this idea, we found that chelating extracellular calcium with EGTA reduced hypoosmotic cell surface expansion (Fig. 1 D).

Cch1 belongs to the family of voltage-gated calcium channels, and the voltage sensor seems to be conserved. In fact, Cch1 mediates a calcium influx as a result of pH increase of the extracellular medium from ∼4 (optimal pH for yeast growth) to ∼7.5 (addition of Tris buffer; Fig. 7 B). This pH increase is expected to depolarize the negative membrane potential of the yeast PM, thereby triggering the Cch1-dependent influx of calcium. We observed a reduced calcium response in *cch1*Δ cells after Tris treatment, indicating that depolarization indeed triggers Cch1-mediated influx of extracellular calcium (remaining calcium likely originates from the vacuole). The maximal GCaMP signal was on average ∼1.5-fold lower in *cch1*Δ cells compared with wild type (quantifications in Fig. 7, A and B).

Concomitant with the calcium influx, we found that the Tris treatment also resulted in a cell surface increase of ∼10% (Fig. 7 C), suggesting that the calcium signal is sufficient to cause cER-to-PM membrane transfer even in the absence of a hypoosmotic shock. Similar to the hypoosmotic-induced cell surface increase, high-pH induced cell surface increase also required the tricalbins (Fig. 7 C). In summary, Cch1 seems to function both as a stretch- and voltage-gated calcium channel that is important for the rapid cell surface expansion during stress conditions.

Both *tcb2/3*Δ and *ist2*Δ mutants exhibited changes in the calcium response to hypoosmotic shock (Fig. 7 A). The response curve showed a much sharper peak compared with wild type, which might either be the result of the higher PM tension predicted in these mutants after hypoosmotic shock or caused by calcium influx through small ruptures of the PM. In addition, *ist2*Δ mutants also exhibited a blinking GCaMP fluorescence, indicating that hypoosmotic stress in this strain produced multiple calcium waves (Fig. 7 A). This finding was consistent with the observed slow cell size increase of this mutant (Fig. 4), indicating multiple rounds of calcium-triggered cER-PM membrane transfer events. Cch1 is known to exhibit calcium-mediated feedback inhibition (Muller et al., 2001), which can explain why the prolonged membrane tension in hypoosmotic-stressed *ist2*Δ does not result in a single, prolonged calcium signal but causes repeated calcium waves.

What is the mechanism for cER-to-PM membrane transport?

With both spheroplasts and walled cells, we observed a surface increase of ∼1% per second, which corresponds to a transfer rate of ∼4 × 10^6 lipids/s (0.4 nm^2 per lipid; 1% of surface area = 8 × 10^5 nm^2; 2 lipid layers). This lipid transfer seems to occur without energy input since depletion of ATP by the addition of NaN_3 and NaF 5 min before treatment did not affect the surface expansion rate during hypoosmotic shock (Fig. 1 D; addition of NaN_3/NaF causes ATP loss within <1 min; [Moharir et al., 2018]). The current models of EPCS function would suggest that this transfer is accomplished by lipid transport proteins. The tricalbin proteins contain SMP domains that have been shown to bind and transport lipids at a rate of <1 lipid/s (in vitro rate; [Yu et al., 2016]). Since there are ∼25,000 Tcb1/2/3 proteins per cell (Wong et al., 2017), each tricalbin would have to transfer ∼160

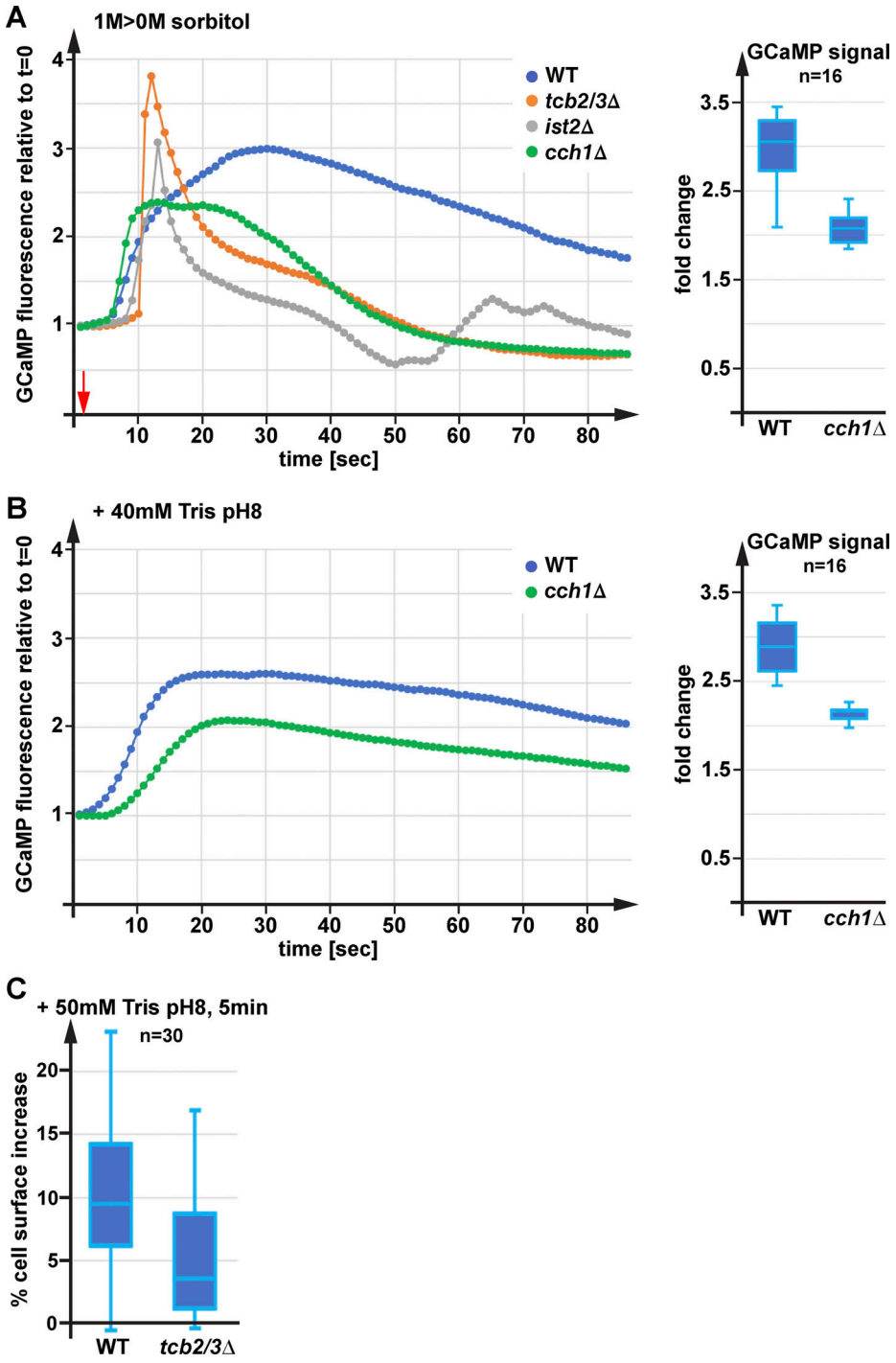

Figure 7. **High membrane tension or loss of membrane potential causes Cch1-mediated calcium influx. (A)** GCaMP-expressing cells (LGY36, MTY5, MTY21, MTY69) were exposed in a microfluidics chamber to a hypoosmotic shock (1 M sorbitol > 0 M sorbitol), and the changes in GCaMP fluorescence were monitored with time-lapse imaging. The red arrow marks the start of cell expansion for all experiments. **(B)** In a microfluidics chamber, cells expressing GCaMP were treated with a medium containing 40 mM Tris pH8 (resulting pH~7.5), and the GCaMP signal was monitored by time-lapse imaging. **(C)** Change in cell surface area caused by the addition of 40 mM Tris pH8 (LGY36, MTY21). The box-and-whisker plots indicate the mean.

lipids/s, >160-times faster than the observed in vitro rate. Therefore, the SMP domains of the tricalbins are unlikely candidates for the massive lipid transfer necessary during hypoosmotic shock. However, we acknowledge the fact that most lipid transfer rates measured in vitro underestimate the true in vivo rates.

A different family of proteins that have been shown to be able to transport ~200 lipids/s are the Vps13-like proteins. Three of these have been localized to the EPCS (Hob2, Csf1, Fmp27; [Neuman et al., 2022; Toulmay et al., 2022]). However, these proteins are rather low expressed and add up to only ~2,000 copies per cell (Wong et al., 2017). As a consequence, the

available Vps13-like proteins would only be able to accommodate ~10% of the necessary lipid transfer rate. Nevertheless, we decided to test the *hob2*Δ, *csf1*Δ, and *fmp27*Δ mutants for potential cell expansion defects. Because the most obvious phenotype we observed with the *tcb2/3*Δ mutant cells was the cytoplasmic pH drop during acute cell expansion (loss of PM barrier function), we performed flow cytometry analysis with yeast expressing the pH sensor pHluorin-mCherry. The resulting data showed that mutations in the Vps13-like proteins had either no phenotype (*hob2*Δ, *hob2*Δ*fmp27*Δ; Fig. 3 D) or phenotypes weaker than those observed in *fps1*Δ (*fmp27*Δ and *csf1*Δ; Fig. 3 D). Vps13-like proteins likely play a role in maintaining proper PM lipid composition, which could explain some of the observed phenotypes.

In the case of *csf1*Δ, the main phenotype was an increase in the "lysed cells" population, which might include cells that ruptured and lost cell wall integrity. However, our gating of the flow cytometry data removed cells with very low mCherry fluorescence and thus might have also removed the ruptured cells. Therefore, we analyzed hypoosmotic-shocked cells expressing the pH sensor pHluorin-mCherry by fluorescence microscopy (using the microfluidics system as in Fig. 2). Quantification of these hypoosmotic-shock experiments confirmed that the main phenotype of *csf1*Δ cells was not the loss of PM barrier function (labeled as lysed cells) but the rupturing of cells (Fig. 3 E), which suggested that *csf1*Δ cells exhibit a weakened cell wall. Consistent with this finding, a recent study implicated Csf1 in the synthesis of GPI-anchored proteins that play an important role in cell wall formation/maintenance (Toulmay et al., 2022). Consistent with the flow cytometry analysis, the microscopy of *hob2*Δ and *fmp27*Δ indicated no or only minor defects in hypoosmotic stress response (Fig. 3 E). In summary, loss of the Vps13-like proteins does not phenocopy the cell expansion defects observed with mutations in the tricalbins, suggesting that these lipid transfer proteins are not required for the delivery of cER membrane to the PM during rapid cell expansion.

Recent cryo-EM analysis of yeast identified membrane peaks in cER sheets, and the presence of these peaks required the tricalbins (see model in Fig. 10 B; [Collado et al., 2019; Hoffmann et al., 2019]). The peaks shorten the distance between cER and PM from ~22 to ~7 nm, and their presence was shown to be important in maintaining cell integrity during heat shock (Collado et al., 2019). Therefore, it was speculated that the peaks represent sites of enhanced tricalbin-mediated lipid transport. With only ~150 peaks per cell, the cER peaks are rather rare structures (Collado et al., 2019). If these peaks are indeed the main sites of lipid transfer during hypoosmotic shock, we would estimate a rate of ~27,000 lipids/s/peak, a transfer rate that could only be accomplished by a direct fusion of the two membranes and not by transfer of individual lipids.

The 7-nm distance between the cER peaks and the PM could be bridged by SNARE proteins, and therefore we considered the possibility that the membrane transfer is accomplished by a SNARE-mediated fusion reaction. Because the PM SNAREs Sso1/2 and the ER SNARE Sec22 have been shown to interact at the EPCS (Weber-Boyvat et al., 2021), we decided to test for cell expansion phenotypes of strains deleted for *SSO1*, *SSO2*, or both *SSO2* and *SEC22*. Flow cytometry and microscopy of these mutant cells expressing the pH sensor showed no increase in cell lysis, no increase in cell ruptures, or decrease in cytoplasmic pH (Fig. 3, D and E), suggesting that these SNAREs are not involved in the proposed fusion reaction or that other SNAREs are able to compensate for the deletions. Alternatively, the fusion could be mediated by a SNARE-independent mechanism.

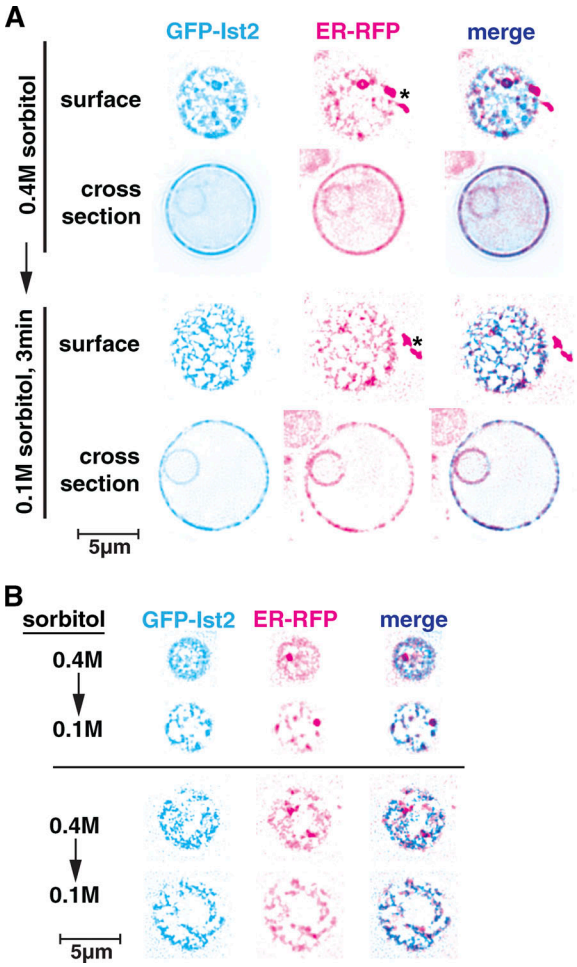

Figure 8. **During cER to PM membrane transport, Ist2 does not get delivered to the cell surface.** Wild-type cells expressing GFP-Ist2 and the ER marker ER-RFP (SEY6210 pMT1 pMT10) were spheroplasted, flushed into the microfluidics chamber, and exposed to hypoosmotic shock (0.4 M sorbitol > 0.1 M sorbitol). **(A and B)** Subpart (A) shows fluorescence microscopy pictures of the surface and cross section of one of these spheroplasts and (B) shows the surface of two additional examples. The star marks cell debris (not part of the analyzed cell).

EPCS-mediated protein transport

Fusion of the cER to the PM would not only provide rapid lipid transport but might also allow for the delivery of proteins from the ER to the cell surface. Because of the large cell expansion, this potential protein transport should be particularly obvious in the case of spheroplast swelling where we observed >50% surface increase. Ist2 is an ER transmembrane protein and is predicted to be in close proximity to the cER peaks. Therefore, we tested if membrane transfer during spheroplast expansion would move a portion of GFP-Ist2 from the cER to the cell

surface. Spheroplasts expressing both GFP-Ist2 and a lumenal ER marker, ER-RFP, showed partial colocalization of these two proteins (Fig. 8 A, additional examples in Fig. 8 B). ER-RFP marked cER colocalized with GFP-Ist2, but some GFP-Ist2-labeled cER sheet exhibited no or very low ER-RFP staining. After the hypoosmotic shock, the expanded spheroplasts had lost the cER sheets (as observed before with ER-pHluorin; see Fig. 5 A) and the two ER markers showed almost perfect colocalization to the tubular cER network (Fig. 8, A and B). This observation was not consistent with an efficient transport of GFP-Ist2 to the cell surface which would have resulted in a more diffuse distribution of this protein at the cell periphery/surface (standard microcopy is not able to visualize cER and PM as discrete structures). In contrast, the data were more consistent with a model in which during spheroplast expansion the lipid transport from the cER to the PM causes the concentration of ER transmembrane proteins into tubular structures.

We considered the possibility that the postulated cER-PM fusion pore might not allow for large multispanning transmembrane proteins, such as Ist2, to be delivered to the cell surface. Therefore, we focused on GPI-anchored proteins, which are translocated as a soluble protein into the lumen of the ER but become attached to the inner leaflet of the ER membrane by the GPI modification. After trafficking to the cell surface via the secretory pathway, most GPI-anchored proteins function in the synthesis and maintenance of the cell wall (Pittet and Conzelmann, 2007). It is important to note that efficient ER exit of GPI-anchored proteins requires the remodeling of the GPI-anchor (Castillon et al., 2011). These remodeling reactions might allow the cell to regulate ER exit and thus maintain an ER pool of the GPI-anchored proteins.

To test if hypoosmotic shock causes the rapid delivery of GPI-anchored proteins to the cell surface, we constructed a fusion protein that replaced the enzymatic domain of the GPI-anchored protein Crh2 (chitin transglycosylase) with the HaloTag. HaloTag is an enzyme that covalently attaches dyes that contain a chloroalkene linker. Depending on the hydrophobicity of the dye, this reaction can be limited to the extracellular surface of the cell (Alexa dyes) or the reaction can occur throughout the cell (membrane permeable TMR dye). HaloTag-based surface labeling of yeast is hampered by the low pH of the growth medium (pH < 4), which required us to buffer the medium to ~pH6.5. In contrast, we found that labeling of the intracellular pool of Crh2-HaloTag with the TMR ligand was only possible at pH~4, a pH at which the carboxy group of the TMR dye is protonated, which allows for easier transmembrane diffusion but inhibits surface labeling. Fig. 9 A shows two examples of cells expressing Crh2-HaloTag that were first labeled with TMR ligand followed by labeling with Alexa488 ligand. Consistent with previously published data (Rodriguez-Pena et al., 2000), the results showed a highly polarized localization for both the ER (TMR labelled) and the surface pool (Alexa488) of the GPI-anchored protein. Cells that were in the G2 phase of the cell cycle showed Crh2-HaloTag localization to the growing bud (intra- and extracellular pool), whereas during cytokinesis, the main pool of Crh2-HaloTag was localized to the site of cell division. In addition, the ER pool of the fusion protein showed

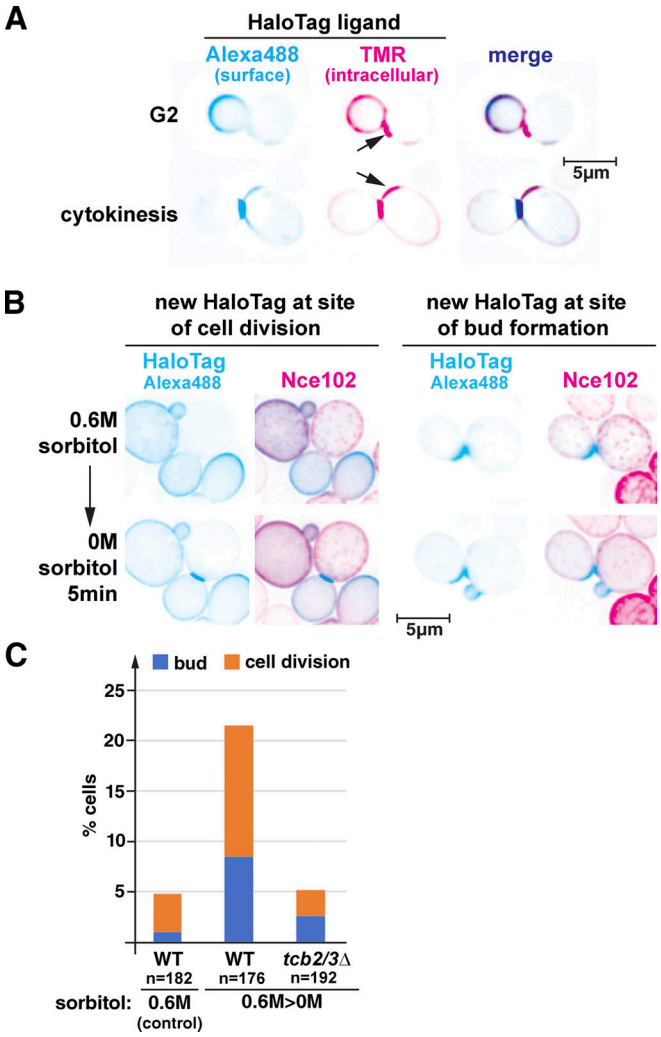

Figure 9. **Hypoosmotic shock causes the delivery of a GPI-anchored protein to the cell surface. (A)** Wild-type yeast expressing a Crh2-HaloTag fusion protein (SEY6210 pLG42) were first stained for 30 min at pH4 (standard growth medium) with the membrane-permeable TMR ligand and were then stained for 5 min at pH6.5 with the hydrophilic Alexa488 ligand. The pictures show examples of cells at two different stages of the cell cycle. **(B)** Cells expressing Nce102-mCherry (cell surface marker) and Crh2-HaloTag (AMY4 pLG42) were grown in the presence of 0.6 M sorbitol, flushed into a microfluidics chamber, and stained with Alexa488 HaloTag ligand for 10 min (first row of pictures). After the switch to hypoosmotic conditions, the cells were stained again with Alexa488 ligand for 5 min (second row of pictures). **(C)** Quantification of the experiments shown in B (AMY4 pLG42, MTY52 pLG42).

localization to the region that likely marked the site for the next budding event (see arrows in Fig. 9 A).

For the hypoosmotic shock experiments, we grew cells expressing Crh2-HaloTag in the presence of 0.6 M sorbitol. These cells were flushed into a microfluidics system and stained with Alexa488 ligand at high concentrations (1 µM) for 10 min (saturated staining). The cells were briefly washed and the control microscopy pictures were taken (see 0.6 M sorbitol in Fig. 9 B). We then performed a hypoosmotic shock and the cells were stained with Alexa488 ligand for 5 min. After a brief wash, the cells were analyzed again by microscopy (see 0 M sorbitol in

Fig. 9 B). The comparison between the two sets of pictures showed that >20% of the cells exhibited new surface staining of Crh2-HaloTag that was not present before the hypoosmotic stress (>2× increase in signal; Fig. 9 C). These new surface pools localized to two distinct places: either a newly formed small bud that rapidly expanded by the hypoosmotic stress or the site of cell division (Fig. 9, B and C). These are also the sites where Crh2-HaloTag was localized intracellularly (see TMR labeling in Fig. 9 A). A control experiment in which we performed the same labeling procedure but without the hypoosmotic shock showed an approximately fourfold lower number of cells with new Crh2-HaloTag surface labeling (Fig. 9 C), which most likely can be attributed to new growth and secretion during the second labeling period. Interestingly, deletion of the tricalbins *TCB2/3* resulted in a similar reduction in new surface labeling as shown for the control experiment. Together, the data indicated that hypoosmotic shock is indeed able to rapidly deliver a new pool of GPI-anchored proteins to the cell surface and that this protein secretion requires the tricalbins. The fact that only a subset of cells showed this secretion of Crh2-HaloTag might be explained by the tight temporal and spatial control of this protein. Crh2 is delivered to the cell surface only in certain phases of the cell cycle and in certain locations where the cell wall is vulnerable to rupture, which could aid in the repair of the stressed cell wall. In any case, our observations with GPI-anchored proteins provide strong support for the proposed cER-PM fusion at contact sites.

Discussion

Yeast osmotic regulation has been extensively studied. Changes in extracellular osmolarity result in changed turgor pressure that is sensed by the HOG and CWI pathways and leads to adaptations by transcriptional regulation. Furthermore, yeast adjusts internal to external osmolarity by either the synthesis or efflux of glycerol, the latter is accomplished via the aquaglyceroporin Fps1 (Luyten et al., 1995). Fig. 10 A summarizes the observations we made with the microfluidics system of hypoosmotic-shocked cells. The shift of growth medium containing 1 M sorbitol to medium without sorbitol (time = 0 s) caused a rapid cell swelling (blue line, increase in cell surface area), indicating that water influx into the cell resulted in increased turgor pressure (black line; predicted, not measured). With a delay of ∼4 s, the cytoplasmic calcium concentration increased, indicating the opening of the calcium channel Cch1 (and vacuolar channels; yellow line). 4 s after the calcium response, we observed a transient drop in cytoplasmic pH, suggesting increased proton influx from the acidic environment. After ∼20 s, the maximal surface area increase is reached. Because of glycerol release and water influx, turgor pressure is predicted to drop to normal levels. It should be noted that this timing of events is based on a limited set of carefully analyzed examples and thus variations might be possible.

The hypoosmotic swelling of yeast occurred within ∼20 s and resulted in a ∼20% increase in cell surface area, which begged the question: how are cells able to add a large amount of membrane to the cell surface within seconds? Our candidate approach identified the tricalbins, also referred to as extended synaptotagmins, as essential factors in the rapid cell surface expansion. Approximately 25% of hypoosmotic-treated *tcb2/3*Δ cells either lost PM barrier function (lysed) or ruptured (loss of both PM and cell wall integrity). An additional 55% of these mutant cells exhibited a pronounced drop in cytoplasmic pH during cell swelling, indicating a partial loss of PM barrier function (Fig. 10 A). Consistent with the presence of defects in the PM, we also observed in these cells a sharp calcium peak that started later during cell swelling (concomitant with the pH drop) and reached higher concentrations than in wild type, which suggested that most of this calcium influx might not have been mediated by Cch1 but by fractures in the PM. With the drop in turgor pressure, the *tcb2/3*Δ mutants reduced their cell size, consistent with the idea that these cells did not add membrane to the cell surface (Fig. 10 A).

The tricalbins are part of the EPCS and function as tethers that keep cER within ∼22 nm of the PM. Furthermore, the SMP domains of the tricalbins have been shown to bind and transfer lipids (Saheki et al., 2016; Yu et al., 2016). However, the phenotypes of tricalbin mutants are generally minor and do not affect cell growth or survival. In fact, mice with deletions in all three tricalbin homologs (deletion of E-Syt1/2/3) exhibit no developmental problems. Most of the phenotypes associated with the loss of the tricalbins were only observed when combined with mutations in other EPCS proteins, and these phenotypes could be complemented by tricalbin constructs that lacked the lipid-binding SMP domain but maintained the ER-PM tether function of the protein. These observations questioned the importance of tricalbin-mediated lipid transfer. However, recent studies found that tricalbins and their lipid transfer activity played an important role in maintaining PM barrier function during heat shock (Collado et al., 2019; Thomas et al., 2022), and we observed dramatic defects in tricalbin mutants in hypoosmotic-induced cell swelling. Both high temperature and high membrane tension cause an increase in membrane fluidity of the PM that threatens the barrier function. Therefore, we propose that the tricalbins act as a stress response system that counters an acute increase in PM fluidity by transferring membrane from the cER to the PM and thus allowing the cell to maintain cell integrity. This membrane transfer is highly efficient and enables yeast spheroplasts to increase their surface area by >50% in less than a minute.

With regard to the mechanism of cER-to-PM membrane transport, the most important observation was the hypoosmotic-induced delivery of the GPI-anchored protein Crh2 to the cell surface. This observation strongly supported the model that at the EPCS, the cER was able to fuse with the PM and deliver both lipids and proteins to the surface. The combined transport of lipids and GPI-anchored proteins is physiological sensible since cell expansion requires not only the addition of lipids to the PM but also a remodeling of the cell wall by GPI-anchored enzymes such as Crh2. It is important to note that we did not observe the hypoosmotic-triggered transport of Ist2 to the cell surface, suggesting that only a specific subset of ER proteins might be able to pass the fusion pore.

A model for the cER-to-PM membrane transport

We proposed that the recently discovered tricalbin-mediated cER peaks (Collado et al., 2019) are sites of stress-induced

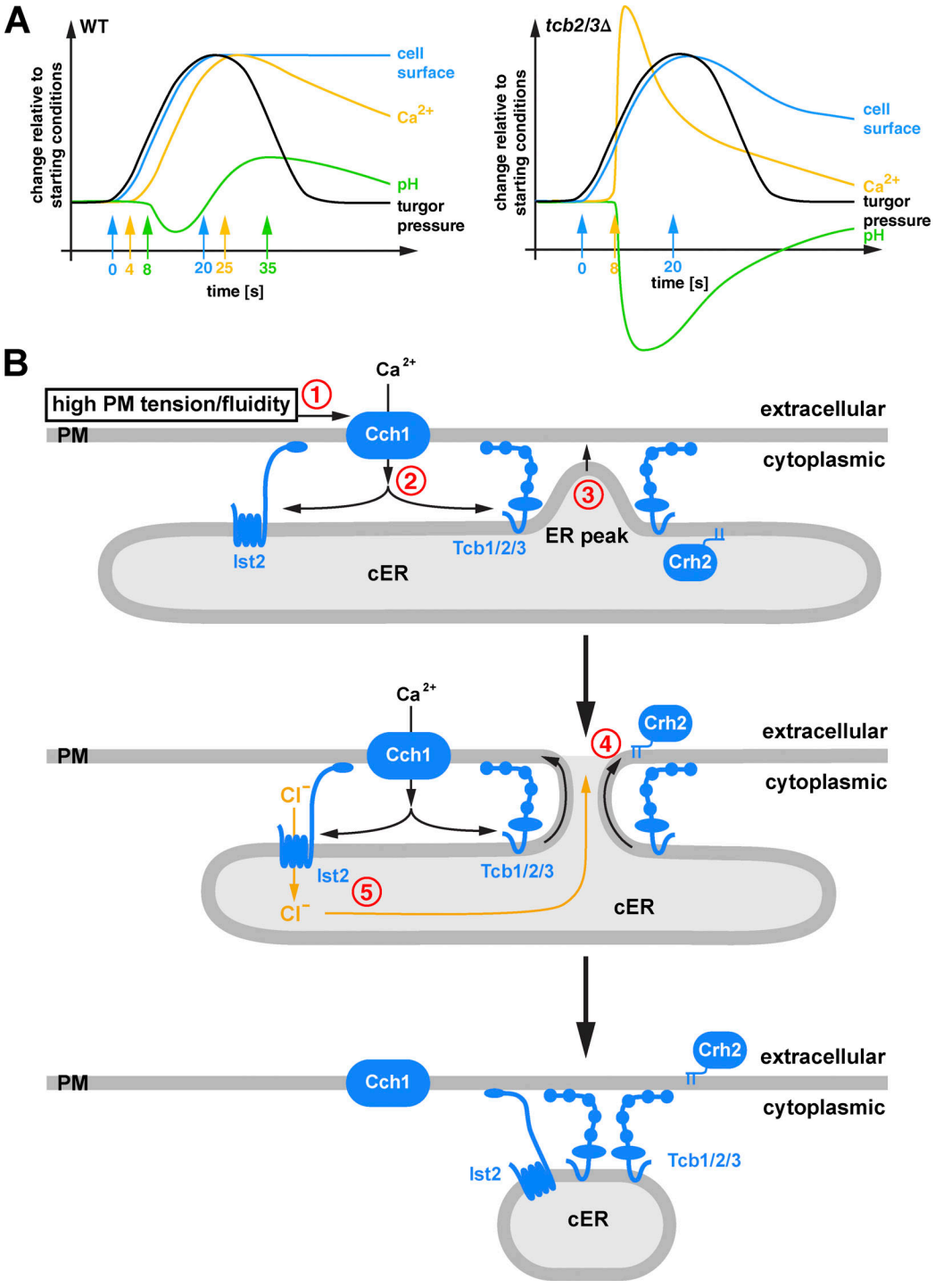

Figure 10. **Summary and interpretation of our observations. (A)** Microfluidics-based analysis of yeast hypoosmotic shock. Time 0 marks the time point at which we observed the beginning of the cell surface increase (blue line). Based on this observed swelling, we predict that the turgor pressure increased shortly before (black line). In wild type, the cytoplasmic calcium increase followed ∼4 s after cell expansion started (yellow line) and another 4 s later the cytoplasmic pH showed a small drop (green line). In contrast, tcb2/3Δ cells exhibited a calcium spike and a dramatic pH drop ∼8 s after cell expansion started. Furthermore, the increased cell size did not remain and when the turgor pressure dropped the mutant cells lost some of their surface expansion. **(B)** Model of the tricalbin-mediated transport of cER membrane to the PM. At cER sheets, the tricalbins form a ring structure that deforms the membrane into ER peaks. High PM fluidity, caused either by high tension or heat-shock, opens the calcium channel Cch1 (step 1). The local influx of calcium (step 2) causes the tricalbins to shorten the distance between the cER and the PM (step 3), thereby bringing the fusogenic ER peak into close proximity to the high-fluidity PM. As a result, the membranes fuse, which allows rapid delivery of ER lipids and the GPI-anchored protein Crh2 to the cell surface (step 4). The tricalbin ring acts as a diffusion barrier for transmembrane proteins and thus prevents the delivery of Ist2 to the cell surface. High-calcium concentrations activate the chloride channel Ist2, which after fusion becomes part of the PM. The resulting secretion of chloride ions (step 5) lowers the membrane potential and as a consequence increases the calcium influx via Cch1 at other fusion sites. Finally, the fusion pore collapses, leaving behind a cER with a reduced lipid/protein ratio and thus a changed morphology.

membrane fusion between the cER and the PM (see model in Fig. 10 B). The cER peaks are rather rare structures of cER sheets (~150/cell; [Collado et al., 2019]) that shorten the distance between the cER and PM from ~22 to ~7 nm. Tcb1/2/3 assemble into heterodimers and larger oligomers (Zanetti et al., 2016) and thus the cER peaks might be formed by a circular arrangement of tricalbins that locally deform the membrane. High PM tension (high PM fluidity) causes an influx of calcium via Cch1 (steps 1 and 2 in Fig. 10 B). High calcium concentrations stabilize the interaction between the tricalbins and the PM, which have been shown to further shorten the distance between the cER peaks and the PM by another 2 nm (step 3, Fig. 10 B; [Collado et al., 2019]). We predict that this narrowing of the cER-PM gap is the trigger for the fusion reaction (step 4, Fig. 10 B).

The PM SNAREs Sso1/2 and the ER SNARE Sec22 have been shown to interact at the EPCS, making these SNAREs good candidates for the proposed fusion reaction. However, our analysis suggested that these SNARE proteins are not involved in the membrane transfer reaction and thus we conclude that either other SNAREs are involved or, our preferred model, that the fusion reaction is SNARE independent. The tip of the cER peak is a highly curved membrane (10 nm diameter, [Collado et al., 2019]) and thus predicted to be unstable and fusogenic. Bringing this highly curved membrane tip in close proximity to a PM that is under high tension could provide a SNARE-independent fusion mechanism.

The lipid-binding SMP domains of the tricalbins might further promote a fusion reaction. In mammalian cells, the tricalbin homologs (E-Syt1/2/3) have been shown to transport diacylglycerol (DAG) from the PM to the ER (Saheki et al., 2016). Because of the lack of a headgroup, DAG is considered a fusogenic lipid (Das and Rand, 1984). Therefore, SMP-mediated DAG transport (under normal growth conditions) might cause local enrichment of DAG both at the cER peaks and the adjacent PM, which would further lower the fusion barrier. Finally, it has been speculated that after calcium influx, the reduced distance between cER peaks and the PM allows for fast SMP-mediated lipid transfer between ER and the PM (Collado et al., 2019). This fast, local lipid transfer might be able to bridge the remaining gap between the membranes and facilitate the fusion of the cER peaks with the PM.

Although our model of cER-PM fusion is speculative, it is the model that best incorporates our observations and previously published data. This model can also explain the role of Ist2 in the cER-PM membrane transfer. Deletion of *IST2* did not block but delayed the membrane transfer from the cER to the PM (Fig. 4), suggesting that Ist2 increases the efficiency of the transfer. Based on sequence comparison, Ist2 has been proposed to function as a calcium-regulated chloride channel (Kunzelmann et al., 2016). Cells use the efflux of chloride ions to depolarize the membrane potential. Our data in Fig. 7 indicated that the calcium channel Cch1 is triggered both by tension and depolarization of the membrane potential and thus Ist2 might function in supporting the opening of Cch1. Consistent with this idea, we observed that *ist2*Δ mutants exhibited a reduced hypoosmotic-triggered calcium influx (Fig. 7 A). However, to be able to depolarize the PM, Ist2 has to be embedded in the PM. Since Ist2 localizes to the cER, the fusion of cER to the PM would be essential to allow Ist2 to lower the membrane potential and thus further activate Cch1 (step 5, Fig. 10 B).

A backup system that bypasses the tricalbins?

Based on our model, the loss of tricalbin function should eliminate the cER-to-PM membrane transfer. Surprisingly, we found a few cases where *tcb2/3*Δ spheroplasts were able to expand during hypoosmotic shock without obvious loss of cell integrity. Furthermore, these spheroplasts exhibited loss of cER, indicating that these few mutant cells were able to transfer membrane from the ER to the PM without Tcb2 and Tcb3. It is possible that Tcb1 alone might maintain some functionality. Alternatively, yeast might have a backup system that can bypass the need for the tricalbins. The PM fractures that seem to form in *tcb2/3*Δ during hypoosmotic expansion (dramatic cytoplasmic pH drop and calcium spike) form membrane edges that are predicted to be highly fusogenic. If the PM tension is not too high, these edges can fuse back together, sealing the fracture. However, when the high tension on the PM does not allow resealing, the edges of the fracture might have the chance to fuse to the nearby cER. This repair might not be efficient but it could represent an emergency backup when other systems fail. In general, yeast is surprisingly resilient to osmotic shocks. Even hypoosmotic-treated *tcb2/3*Δ mutants that exhibited cell lysis and thus a cytoplasmic pH below 5 were able to restore normal pH within ~5 min and remained viable. Only cells that lost cell wall integrity (ruptured cells) also lost viability. Therefore, as long as the cell wall remains intact, yeast is able to recover even after complete loss of PM barrier function.

PS exposure and evolutionary conservation of the ER-PM membrane transport

As a consequence of the cER-to-PM membrane transfer, we observed the exposure of PS at the cell surface, a phospholipid that exclusively localizes to the cytoplasmic leaflet of the PM under normal conditions. Based on our model, we could predict that this pool of surface-exposed PS originated from the lumenal leaflet of the cER membrane. An alternative explanation is that the PS exposure would be the activation of scramblases that might aid in the rapid cell expansion. Among the best-studied scramblases are the mammalian TMEM16 proteins, which are homologs to yeast Ist2. TMEM16F has been studied extensively for its role in calcium-triggered PS exposure and cell surface expansion, particularly in platelets (Yang et al., 2012; Suzuki et al., 2010; Bricogne et al., 2019). Although the proposed mechanisms by which TMEM16F performs these functions differ from our model, both of these roles of TMEM16F fit well with our observed function of the EPCS in cER-to-PM membrane transport. Therefore, it is possible that analogous to Ist2, TMEM16F is involved in the delivery of ER membrane to the cell surface, which would suggest that at least part of the TMEM16F-mediated PS exposure is not due to scramblase activity but the surface exposure of ER membrane. In the case of yeast, Ist2 was not essential for hypoosmotic-triggered PS exposure (Fig. 6), supporting the notion that Ist2 is likely not a scramblase.

Beyond platelet activation, there is additional published evidence for the conserved function of the Ist2/TMEM16 proteins in ER-to-PM membrane transport. For example, in HEK293 cells, the addition of a calcium ionophore or the activation of mechanosensitive calcium channels causes within seconds TMEM16F-dependent expansion of the cell surface by >50% and the concomitant exposure of PS (Deisl et al., 2021). In mouse lens cells, TMEM16A has been shown to secrete chloride ions in response to a hypoosmotic shock (Ebihara et al., 2022). Furthermore, the delivery of TMEM16A to the cell surface and its function as a chloride channel was found to be dependent on the tricalbin-homolog E-Syt1 (Lerias et al., 2018), suggesting that in this case, the cER-PM fusion might deliver not only membrane but also TMEM16A to the cell surface. The mammalian system is clearly more complex, indicated by the expression of 10 different TMEM16 proteins with different locations. Some of the TMEM16 proteins are mainly surface localized (e.g., TMEM16F), whereas others are found, similar to Ist2, mainly in the ER and the EPCS (e.g., TMEM16H; [Jha et al., 2019]). In addition, compared with Ist2, TMEM16F and other proteins from this family seem to play a more dominant role in the proposed ER-PM membrane transfer. Current literature does not contain evidence for the role of the mammalian E-Syt proteins in rapid cell expansion. However, studies in plants identified the tricalbin-homolog SYT1 as an important factor in maintaining cell integrity during acute PM stress, such as freezing, osmotic, and mechanical stress (Ruiz-Lopez et al., 2021; Schapire et al., 2008), suggesting a PM-protective role similar to that of the tricalbins.

In summary, our analysis identified the EPCS proteins Tcb2/3 and Ist2 as an important system that allows for large PM expansion in a timescale of seconds. EPCS activity counters the acute PM tension that occurs during hypoosmotic shock by transferring the membrane from the cER to the PM and thus allowing the cell to maintain cell integrity. We propose that the tricalbins mediate a direct fusion of the cER with the PM at ER peaks, thereby allowing for rapid transfer of membrane and certain proteins to the cell surface. The low number of ER peaks compared with the large number of tricalbin proteins indicates that most tricalbins are not involved in this proposed fusion reaction but have additional functions, as described in previous publications (e.g., [Saheki et al., 2016; Collado et al., 2019; Hoffmann et al., 2019; Thomas et al., 2022]).

Materials and methods

Strains, media, and plasmids

Yeast strains were grown at 30°C in synthetic dextrose medium (SD; yeast nitrogen base, 2% glucose), either in the presence of all amino acids and essential supplements (SD_{comp}) or in case of plasmid selection lacking certain amino acids/supplements. The yeast strains and plasmids used in this study are listed in Table 1. To induce expression from *CUP1* promoter-driven constructs we added 0.1 mM $CuSO_4$ to the medium. Approximately 30 min before the experiment we switched the strains to $CuSO_4$ free medium to avoid any oxidative lipid damage. Chromosomal gene tagging or deletion was performed by homologous recombination (Longtine et al., 1998). The modifications were confirmed by PCR analysis.

Fluorescence microscopy

For most of the fluorescence microscopy (Olympus deconvolution microscope, 100× objective, ORCA-Flash4.0 camera), we used a microfluidics system (CellASIC ONIX; Millipore Sigma) at 30°C and with a constant flow of medium (4 psi). All cells were imaged at mid-log phase (OD_{600} ~0.8). To minimize changes in growth parameters, the medium for the microfluidics system was obtained by centrifugation of the culture used for analysis (conditioned medium). To quantify changes in cell diameter and surface area from the mother and bud, Fiji was used to threshold, binarize, and stack images taken before and 2 min after hypoosmotic treatment (Schindelin et al., 2012). Regions of interest were then targeted and measured by Fiji (Fig. 1, A and B). Further cell surface quantifications were based on measured cell diameters and the assumption that the yeast cells are spherical (exception: Fig. 1, A and B; see text). Quantifications of pHluorin, GCAMP, and mCherry signals were performed manually using the Olympus microscope software. Changes in the size of the cER were determined by quantifying the pixel number of ER-pHluorin marked cER in a single optical section of the cell cortex using the Adobe Photoshop magic wand tool.

Plating assay

Yeast cultures were grown at 30°C in SD_{comp} +1 M sorbitol medium to an OD_{600} of 1.0. The cells were harvested by centrifugation (5 min at 7,000 rpm), resuspended in a prewarmed medium containing either 1 M sorbitol (control) or in a medium without sorbitol (hypoosmotic), and incubated at 30°C for 5 min. The cells were serially diluted, spread on YPD plates using a glass rod, and incubated at 30°C for 48 h before colonies were counted.

Spheroplasting and annexin-V staining

For spheroplasting, a 5 ml yeast culture was harvested at mid-log phase and then incubated in 1 ml softening buffer (100 mM Tris pH9.4 + 10 mM DTT) at room temperature for 10 min. The cells were centrifuged and resuspended in 1 ml spheroplasting medium (SD_{comp} + 40 mM MES pH6.5 + sorbitol as indicated [0.8 or 0.4 M]) containing 10 µl of 50 mg/ml zymolyase. The cells were spheroplasted for 45 min at 30°C. The spheroplasts were washed with the spheroplasting medium and then either used for a microfluidics experiment or for annexin-V staining. For the annexin-V staining, the spheroplasts were pelleted and resuspended at 30°C in a labeling medium (spheroplast medium +2 mM $CaCl_2$ +5 mM NaF +5 mM NaN_3) containing either 0.8 M sorbitol (control) or in a labeling medium with 0.1 M sorbitol (hypoosmotic). The spheroplasts were incubated for 2 min at 30°C. At room temperature, the spheroplasts were then stained with annexin-V conjugated to Alexa Fluor 488 (Thermo Fisher Scientific) and imaged by fluorescence microscopy.

Flow cytometry

Yeast strains containing the plasmid pMB517 were grown to the mid-log phase in a medium containing 0.1 mM $CuSO_4$ (to induce

Table 1. **Strains and plasmid**

Strains	Descriptive name	Genotype or description	Reference or source
SEY6210	WT	*MATα leu2-3,112 ura3-52 his3-Δ200 trp1-Δ901 lys2-801 suc2-Δ9 GAL*	Robinson et al. (1988)
MTY2	*ist2Δ*	SEY6210, *IST2::TRP1*	This study
MTY18	*tcb2/3Δ*	SEY6210, *TCB2::HIS3, TCB3::TRP1*	This study
AMY4	*NCE102-mCherry*	SEY6210, *NCE102-mCherry, KANMX6*	Moharir et al. (2018)
MTY81	*fps1Δ, NCE102-mCherry*	AMY4, *FPS1::TRP1, NCE102-mCherry, KANMX6*	This study
MTY55	*pil1Δ, NCE102-mCherry*	AMY4, *PIL1::TRP1, NCE102-mCherry, KANMX6*	This study
MTY52	*tcb2/3Δ, NCE102-mCherry*	AMY4, *TCB3::TRP1, TCB2::HIS3, NCE102-mCherry, KANMX6*	This study
MTY83	*tcb2/3Δpil1Δ, NCE102-mCherry*	MTY52, PIL1::hphMX, *TCB3::TRP1, TCB2::HIS3, NCE102-mCherry, KANMX6*	This study
MTY47	*ist2Δ, NCE102-mCherry*	AMY4, *IST2::TRP1, NCE102-mCherry, KANMX6*	This study
MTY68	*cch1Δ, NCE102-mCherry*	AMY4, *CCH1::TRP1, NCE102-mCherry, KANMX6*	This study
AMY42	*pil1Δ*	SEY6210, *PIL1::KANMX6*	Moharir et al. (2018)
LGY83	*fps1Δ*	SEY6210, *FPS1::TRP1*	This study
AMY56	*cch1Δ*	SEY6210, *CCH1::TRP1*	This study
MTY89	*hob2Δ*	SEY6210, *HOB2::TRP1*	This study
MTY7	*sso2Δ*	SEY6210, *SSO2::TRP1*	This study
MTY86	*sso2Δsec22Δ*	SEY6210, *SSO2::TRP1, SEC22::HIS3*	This study
MTY91	*csf1Δ*	SEY6210, *CSF1::TRP1*	This study
MTY11	*sso1Δ*	SEY6210, *SSO1::TRP1*	This study
STY11	*fmp27Δ*	SEY6210, *FMP27::KANMX6*	This study
LGY36	*GCaMP*	SEY6210, *ura3::GPDp-GCaMP3-ADH1t-KANMX4*	This study
MTY5	*ist2Δ, GCaMP*	SEY6210, *IST2::TRP1, ura3::GPDp-GCaMP3-ADH1t-KANMX4*	This study
MTY21	*tcb2/3Δ, GCaMP*	SEY6210, *TCB2::HIS3, TCB3::TRP1, ura3::GPDp-GCaMP3-ADH1t-KANMX4*	This study
MTY69	*cch1, GCaMP*	SEY6210, *CCH1::TRP1, ura3::GPDp-GCaMP3-ADHt-KANMX4*	This study
MTY93	*hob2Δfmp27Δ*	SEY6210, *FMP27::KANMX4, HOB2::TRP1*	This study
Plasmids			
pMB517	P(*CUP1*)-*sepHluorin-mCherry*	URA3 (pRS416) P(CUP1)-sepHluorin-mCherry	Moharir et al. (2018)
MRV66	ER-pHluorin	p426MET25_SSKar2-sfpHluorin-HDEL	Reifenrath and Boles (2018)
pMT1	P(*CUP1*)-GFP-IST2	URA3 (pRS426) P(*CUP1*)-*GFP-IST2*	This study
pSAB366	*GCaMP3*	*pRS306K*-GPD1p-GCaMP3-ADH1t-KANMX4	Carbo et al. (2017)
pRS305-dsRED-HDEL	dsRED-HDEL	LEU2 *(pRS305)-dsRED-HDEL*	Mike Henne
pMT10	ER-RFP	LEU2 *(pRS415)*-dsRED-HDEL	This study
pLG42	P(*CUP1*)-*CRH2*-HaloTag	URA3 (pRS426) P(CUP1)- *CRH2*-HaloTag	This study

the promoter) and 1 M sorbitol. To avoid lipid oxidation, 30 min before the analysis, the cells were moved into a new growth medium with 1 M sorbitol but lacking $CuSO_4$. The cells were harvested by centrifugation (45 s at 5,500 rpm) and resuspended either in a medium containing 1 M sorbitol (control) or in a medium without sorbitol (hypoosmotic). During resuspending, the cells and the medium were kept at 30°C. Immediately after resuspending, the strains were analyzed using the CytoFlex S flow cytometer (Beckman Coulter). The pHluorin and mCherry fluorescence data of ∼200,000 events were collected for each sample. Events with mCherry fluorescence <550 units were discarded and the data was analyzed using the CytExpert software package.

HaloTag experiments

The Crh2-HaloTag fusion construct contained the following elements: *CUP1* promoter, 1–75 bp *CRH2*, HaloTag (Promega), 991-end *CRH2*, 3′ termination/polyA sequence. The resulting plasmid, pLG42, was transformed into yeast, and the expression of the Crh2-HaloTag fusion was induced by adding 0.1 mM $CuSO_4$ to the growth medium. In case of staining with the membrane-permeable TMR HaloTag ligane (Promega), we added the dye at 200 nM to the growing cells for 30 min. For the staining with the non-permeable Alexa488 ligand, we grew the cells in medium buffered to pH6.5 (50 mM MES), flushed the cells into the microfluidics chamber, and added the Alexa488 ligand at 1 µM in pH6.5 medium for 5–10 min. The hypoosmotic stress experiments with Alexa488 ligand were performed with a switch from 0.6 M sorbitol to no sorbitol in the medium. 0.6 M sorbitol was chosen because 1 M sorbitol in combination with pH6.5 medium resulted in very poor growth.

Online supplemental material

Video 1 in Supplemental Material shows time-lapse imaging (1 frame/3 s) of a spheroplast (AMY4 expressing MRV66) observed by epifluorescence microscopy in the microfluidics chamber during the switch from high to low osmolarity medium (1 M > 0 M sorbitol). The movie has been sped up 3× (actual duration is 120 s).

Data availability

Microscopy images that are the basis for the analyses shown in Figs. 1, 2, 4, 5, 6, 7, 8, 9, and 10 are available from the corresponding author upon reasonable request. The data underlying Fig. 3 are available in the published article.

Acknowledgments

We thank Jasmine Phan for the critical reading of this document.

The research was supported by a grant from the National Institutes of Health (National Institute of General Medical Sciences R01 GM123147 to M. Babst).

Author contributions: M. Smith: Conceptualization, Data curation, Formal analysis, Investigation, Methodology, Project administration, Validation, Visualization, Writing—original draft, Writing—review & editing, L. Gay: Investigation, M. Babst: Conceptualization, Formal analysis, Funding acquisition, Investigation, Methodology, Project administration, Supervision, Validation, Visualization, Writing—original draft, Writing—review & editing.

Disclosures: The authors declare no competing interests exist.

Submitted: 28 August 2023
Revised: 16 July 2024
Accepted: 27 August 2024

References

Apodaca, G. 2004. The uroepithelium: Not just a passive barrier. *Traffic*. 5: 117–128. https://doi.org/10.1046/j.1600-0854.2003.00156.x

Appadurai, D., L. Gay, A. Moharir, M.J. Lang, M.C. Duncan, O. Schmidt, D. Teis, T.N. Vu, M. Silva, E.M. Jorgensen, and M. Babst. 2020. Plasma membrane tension regulates eisosome structure and function. *Mol. Biol. Cell*. 31:287–303. https://doi.org/10.1091/mbc.E19-04-0218

Batiza, A.F., T. Schulz, and P.H. Masson. 1996. Yeast respond to hypotonic shock with a calcium pulse. *J. Biol. Chem*. 271:23357–23362. https://doi.org/10.1074/jbc.271.38.23357

Berchtold, D., M. Piccolis, N. Chiaruttini, I. Riezman, H. Riezman, A. Roux, T.C. Walther, and R. Loewith. 2012. Plasma membrane stress induces relocalization of Slm proteins and activation of TORC2 to promote sphingolipid synthesis. *Nat. Cell Biol*. 14:542–547. https://doi.org/10.1038/ncb2480

Bricogne, C., M. Fine, P.M. Pereira, J. Sung, M. Tijani, Y. Wang, R. Henriques, M.K. Collins, and D.W. Hilgemann. 2019. TMEM16F activation by Ca^{2+} triggers plasma membrane expansion and directs PD-1 trafficking. *Sci. Rep*. 9:619. https://doi.org/10.1038/s41598-018-37056-x

Carbó, N., N. Tarkowski, E.P. Ipiña, S.P. Dawson, and P.S. Aguilar. 2017. Sexual pheromone modulates the frequency of cytosolic Ca^{2+} bursts in Saccharomyces cerevisiae. *Mol. Biol. Cell*. 28:501–510. https://doi.org/10.1091/mbc.e16-07-0481

Castillon, G.A., A. Aguilera-Romero, J. Manzano-Lopez, S. Epstein, K. Kajiwara, K. Funato, R. Watanabe, H. Riezman, and M. Muñiz. 2011. The yeast p24 complex regulates GPI-anchored protein transport and quality control by monitoring anchor remodeling. *Mol. Biol. Cell*. 22: 2924–2936. https://doi.org/10.1091/mbc.e11-04-0294

Collado, J., M. Kalemanov, F. Campelo, C. Bourgoint, F. Thomas, R. Loewith, A. Martínez-Sánchez, W. Baumeister, C.J. Stefan, and R. Fernández-Busnadiego. 2019. Tricalbin-mediated contact sites control ER curvature to maintain plasma membrane integrity. *Dev. Cell*. 51:476–487.e7. https://doi.org/10.1016/j.devcel.2019.10.018

Das, S., and R.P. Rand. 1984. Diacylglycerol causes major structural transitions in phospholipid bilayer membranes. *Biochem. Biophys. Res. Commun*. 124:491–496. https://doi.org/10.1016/0006-291X(84)91580-8

Deisl, C., D.W. Hilgemann, R. Syeda, and M. Fine. 2021. TMEM16F and dynamins control expansive plasma membrane reservoirs. *Nat. Commun*. 12:4990. https://doi.org/10.1038/s41467-021-25286-z

Douglas, L.M., and J.B. Konopka. 2014. Fungal membrane organization: The eisosome concept. *Annu. Rev. Microbiol*. 68:377–393. https://doi.org/10.1146/annurev-micro-091313-103507

Ebihara, L., P. Acharya, and J.J. Tong. 2022. Mechanical stress modulates calcium-activated-chloride currents in differentiating lens cells. *Front. Physiol*. 13:814651. https://doi.org/10.3389/fphys.2022.814651

Eisenberg-Bord, M., N. Shai, M. Schuldiner, and M. Bohnert. 2016. A tether is a tether is a tether: Tethering at membrane contact sites. *Dev. Cell*. 39: 395–409. https://doi.org/10.1016/j.devcel.2016.10.022

Falzone, M.E., M. Malvezzi, B.C. Lee, and A. Accardi. 2018. Known structures and unknown mechanisms of TMEM16 scramblases and channels. *J. Gen. Physiol*. 150:933–947. https://doi.org/10.1085/jgp.201711957

Fernández-Busnadiego, R., Y. Saheki, and P. De Camilli. 2015. Three-dimensional architecture of extended synaptotagmin-mediated endoplasmic reticulum-plasma membrane contact sites. *Proc. Natl. Acad. Sci. USA*. 112:E2004–E2013. https://doi.org/10.1073/pnas.1503191112

Gatta, A.T., and T.P. Levine. 2017. Piecing together the patchwork of contact sites. *Trends Cell Biol*. 27:214–229. https://doi.org/10.1016/j.tcb.2016.08.010

Hoffmann, P.C., T.A.M. Bharat, M.R. Wozny, J. Boulanger, E.A. Miller, and W. Kukulski. 2019. Tricalbins contribute to cellular lipid flux and form curved ER-PM contacts that are bridged by rod-shaped structures. *Dev. Cell*. 51:488–502.e8. https://doi.org/10.1016/j.devcel.2019.09.019

Hohmann, S. 2002. Osmotic stress signaling and osmoadaptation in yeasts. *Microbiol. Mol. Biol. Rev.* 66:300–372. https://doi.org/10.1128/MMBR.66.2.300-372.2002

Jha, A., W.Y. Chung, L. Vachel, J. Maleth, S. Lake, G. Zhang, M. Ahuja, and S. Muallem. 2019. Anoctamin 8 tethers endoplasmic reticulum and plasma membrane for assembly of Ca^{2+} signaling complexes at the ER/PM compartment. *EMBO J.* 38:e101452. https://doi.org/10.15252/embj.2018101452

Kunzelmann, K., I. Cabrita, P. Wanitchakool, J. Ousingsawat, L. Sirianant, R. Benedetto, and R. Schreiber. 2016. Modulating Ca^{2+} signals: A common theme for TMEM16, Ist2, and TMC. *Pflugers Arch.* 468:475–490. https://doi.org/10.1007/s00424-015-1767-4

Le Roux, A.L., X. Quiroga, N. Walani, M. Arroyo, and P. Roca-Cusachs. 2019. The plasma membrane as a mechanochemical transducer. *Philos. Trans. R. Soc. Lond. B Biol. Sci.* 374:20180221. https://doi.org/10.1098/rstb.2018.0221

Lérias, J.R., M.C. Pinto, H.M. Botelho, N.T. Awatade, M.C. Quaresma, I.A.L. Silva, P. Wanitchakool, R. Schreiber, R. Pepperkok, K. Kunzelmann, and M.D. Amaral. 2018. A novel microscopy-based assay identifies extended synaptotagmin-1 (ESYT1) as a positive regulator of anoctamin 1 traffic. *Biochim. Biophys. Acta Mol. Cell Res.* 1865:421–431. https://doi.org/10.1016/j.bbamcr.2017.11.009

Longtine, M.S., A. McKenzie III, D.J. Demarini, N.G. Shah, A. Wach, A. Brachat, P. Philippsen, and J.R. Pringle. 1998. Additional modules for versatile and economical PCR-based gene deletion and modification in Saccharomyces cerevisiae. *Yeast*. 14:953–961. https://doi.org/10.1002/(SICI)1097-0061(199807)14:10<953::AID-YEA293>3.0.CO;2-U

Luyten, K., J. Albertyn, W.F. Skibbe, B.A. Prior, J. Ramos, J.M. Thevelein, and S. Hohmann. 1995. Fps1, a yeast member of the MIP family of channel proteins, is a facilitator for glycerol uptake and efflux and is inactive under osmotic stress. *EMBO J.* 14:1360–1371. https://doi.org/10.1002/j.1460-2075.1995.tb07122.x

Manford, A.G., C.J. Stefan, H.L. Yuan, J.A. Macgurn, and S.D. Emr. 2012. ER-to-plasma membrane tethering proteins regulate cell signaling and ER morphology. *Dev. Cell*. 23:1129–1140. https://doi.org/10.1016/j.devcel.2012.11.004

Moharir, A., L. Gay, D. Appadurai, J. Keener, and M. Babst. 2018. Eisosomes are metabolically regulated storage compartments for APC-type nutrient transporters. *Mol. Biol. Cell*. 29:2113–2127. https://doi.org/10.1091/mbc.E17-11-0691

Moharir, A., L. Gay, and M. Babst. 2022. Mitochondrial energy metabolism regulates the nutrient import activity and endocytosis of APC transporters. *FEBS Lett.* 596:1111–1123. https://doi.org/10.1002/1873-3468.14314

Muller, E.M., E.G. Locke, and K.W. Cunningham. 2001. Differential regulation of two Ca(2+) influx systems by pheromone signaling in Saccharomyces cerevisiae. *Genetics*. 159:1527–1538. https://doi.org/10.1093/genetics/159.4.1527

Neuman, S.D., J.R. Jorgensen, A.T. Cavanagh, J.T. Smyth, J.E. Selegue, S.D. Emr, and A. Bashirullah. 2022. The Hob proteins are novel and conserved lipid-binding proteins at ER-PM contact sites. *J. Cell Sci.* 135:jcs259086. https://doi.org/10.1242/jcs.259086

Parton, R.G. 2018. Caveolae: Structure, function, and relationship to disease. *Annu. Rev. Cell Dev. Biol.* 34:111–136. https://doi.org/10.1146/annurev-cellbio-100617-062737

Pittet, M., and A. Conzelmann. 2007. Biosynthesis and function of GPI proteins in the yeast Saccharomyces cerevisiae. *Biochim. Biophys. Acta*. 1771:405–420. https://doi.org/10.1016/j.bbalip.2006.05.015

Pontes, B., P. Monzo, and N.C. Gauthier. 2017. Membrane tension: A challenging but universal physical parameter in cell biology. *Semin. Cell Dev. Biol.* 71:30–41. https://doi.org/10.1016/j.semcdb.2017.08.030

Reifenrath, M., and E. Boles. 2018. A superfolder variant of pH-sensitive pHluorin for in vivo pH measurements in the endoplasmic reticulum. *Sci. Rep.* 8:11985. https://doi.org/10.1038/s41598-018-30367-z

Robinson, J.S., D.J. Klionsky, L.M. Banta, and S.D. Emr. 1988. Protein sorting in Saccharomyces cerevisiae: Isolation of mutants defective in the delivery and processing of multiple vacuolar hydrolases. *Mol. Cell. Biol.* 8:4936–4948. https://doi.org/10.1128/mcb.8.11.4936-4948.1988

Rodríguez-Peña, J.M., V.J. Cid, J. Arroyo, and C. Nombela. 2000. A novel family of cell wall-related proteins regulated differently during the yeast life cycle. *Mol. Cell. Biol.* 20:3245–3255. https://doi.org/10.1128/MCB.20.9.3245-3255.2000

Ruiz-Lopez, N., J. Pérez-Sancho, A.E. Del Valle, R.P. Haslam, S. Vanneste, R. Catalá, C. Perea-Resa, D.V. Damme, S. García-Hernández, A. Albert, et al. 2021. Synaptotagmins at the endoplasmic reticulum-plasma membrane contact sites maintain diacylglycerol homeostasis during abiotic stress. *Plant Cell*. 33:2431–2453. https://doi.org/10.1093/plcell/koab122

Saheki, Y., X. Bian, C.M. Schauder, Y. Sawaki, M.A. Surma, C. Klose, F. Pincet, K.M. Reinisch, and P. De Camilli. 2016. Control of plasma membrane lipid homeostasis by the extended synaptotagmins. *Nat. Cell Biol.* 18:504–515. https://doi.org/10.1038/ncb3339

Schapire, A.L., B. Voigt, J. Jasik, A. Rosado, R. Lopez-Cobollo, D. Menzel, J. Salinas, S. Mancuso, V. Valpuesta, F. Baluska, and M.A. Botella. 2008. Arabidopsis synaptotagmin 1 is required for the maintenance of plasma membrane integrity and cell viability. *Plant Cell*. 20:3374–3388. https://doi.org/10.1105/tpc.108.063859

Schindelin, J., I. Arganda-Carreras, E. Frise, V. Kaynig, M. Longair, T. Pietzsch, S. Preibisch, C. Rueden, S. Saalfeld, B. Schmid, et al. 2012. Fiji: An open-source platform for biological-image analysis. *Nat. Methods*. 9:676–682. https://doi.org/10.1038/nmeth.2019

Schulz, T.A., and C.E. Creutz. 2004. The tricalbin C2 domains: Lipid-binding properties of a novel, synaptotagmin-like yeast protein family. *Biochemistry*. 43:3987–3995. https://doi.org/10.1021/bi036082w

Sclip, A., T. Bacaj, L.R. Giam, and T.C. Südhof. 2016. Extended synaptotagmin (ESyt) triple knock-out mice are viable and fertile without obvious endoplasmic reticulum dysfunction. *PLoS One*. 11:e0158295. https://doi.org/10.1371/journal.pone.0158295

Scorrano, L., M.A. De Matteis, S. Emr, F. Giordano, G. Hajnóczky, B. Kornmann, L.L. Lackner, T.P. Levine, L. Pellegrini, K. Reinisch, et al. 2019. Coming together to define membrane contact sites. *Nat. Commun.* 10:1287. https://doi.org/10.1038/s41467-019-09253-3

Suzuki, J., M. Umeda, P.J. Sims, and S. Nagata. 2010. Calcium-dependent phospholipid scrambling by TMEM16F. *Nature*. 468:834–838. https://doi.org/10.1038/nature09583

Thomas, F.B., D.J. Omnus, J.M. Bader, G.H. Chung, N. Kono, and C.J. Stefan. 2022. Tricalbin proteins regulate plasma membrane phospholipid homeostasis. *Life Sci. Alliance*. 5:e202201430. https://doi.org/10.26508/lsa.202201430

Toulmay, A., F.B. Whittle, J. Yang, X. Bai, J. Diarra, S. Banerjee, T.P. Levine, A. Golden, and W.A. Prinz. 2022. Vps13-like proteins provide phosphatidylethanolamine for GPI anchor synthesis in the ER. *J. Cell Biol.* 221:e202111095. https://doi.org/10.1083/jcb.202111095

Tremblay, M.G., and T. Moss. 2016. Loss of all 3 Extended Synaptotagmins does not affect normal mouse development, viability or fertility. *Cell Cycle*. 15:2360–2366. https://doi.org/10.1080/15384101.2016.1203494

Tsuji, T., J. Cheng, T. Tatematsu, A. Ebata, H. Kamikawa, A. Fujita, S. Gyobu, K. Segawa, H. Arai, T. Taguchi, et al. 2019. Predominant localization of phosphatidylserine at the cytoplasmic leaflet of the ER, and its TMEM16K-dependent redistribution. *Proc. Natl. Acad. Sci. USA*. 116:13368–13373. https://doi.org/10.1073/pnas.1822025116

Weber-Boyvat, M., T. Trimbuch, S. Shah, J. Jäntti, V.M. Olkkonen, and C. Rosenmund. 2021. ORP/Osh mediate cross-talk between ER-plasma membrane contact site components and plasma membrane SNAREs. *Cell. Mol. Life Sci.* 78:1689–1708. https://doi.org/10.1007/s00018-020-03604-w

West, M., N. Zurek, A. Hoenger, and G.K. Voeltz. 2011. A 3D analysis of yeast ER structure reveals how ER domains are organized by membrane curvature. *J. Cell Biol.* 193:333–346. https://doi.org/10.1083/jcb.201011039

Wong, L.H., A. Čopič, and T.P. Levine. 2017. Advances on the transfer of lipids by lipid transfer proteins. *Trends Biochem. Sci.* 42:516–530. https://doi.org/10.1016/j.tibs.2017.05.001

Yang, H., A. Kim, T. David, D. Palmer, T. Jin, J. Tien, F. Huang, T. Cheng, S.R. Coughlin, Y.N. Jan, and L.Y. Jan. 2012. TMEM16F forms a Ca^{2+}-activated cation channel required for lipid scrambling in platelets during blood coagulation. *Cell*. 151:111–122. https://doi.org/10.1016/j.cell.2012.07.036

Yu, H., Y. Liu, D.R. Gulbranson, A. Paine, S.S. Rathore, and J. Shen. 2016. Extended synaptotagmins are Ca^{2+}-dependent lipid transfer proteins at membrane contact sites. *Proc. Natl. Acad. Sci. USA*. 113:4362–4367. https://doi.org/10.1073/pnas.1517259113

Zanetti, M.N., O.D. Bello, J. Wang, J. Coleman, Y. Cai, C.V. Sindelar, J.E. Rothman, and S.S. Krishnakumar. 2016. Ring-like oligomers of Synaptotagmins and related C2 domain proteins. *Elife*. 5:e17262. https://doi.org/10.7554/eLife.17262

JCB

Supplemental material

Video 1. **Time-lapse imaging (1 frame per 3 s) of a wild-type spheroplast expressing Nce102-mCherry (red channel; PM marker) and ER-pHluorin (green channel; ER marker) (AMY4 MRV66).** The spheroplast was observed by epifluorescence microscopy in a microfluidics chamber that was switched from a growth medium containing 0.4 M sorbitol to a medium with 0.1 M sorbitol (hypoosmotic shock). The video is sped up threefold (actual duration is 120 s).